Transcriptional regulation and repressive condensates modulate a proliferative-invasive cellular switch *in vivo*

Authors: Taylor N. Medwig-Kinney[1†*], Brian A. Kinney[2†], Michael A. Q. Martinez[1], Callista Yee[3], Sydney S. Sirota[1‡], Angelina A. Mullarkey[1], Neha Somineni[1§], Justin Hippler[1,4#], Wan Zhang[1], Kang Shen[3], Christopher M. Hammell[2], Ariel M. Pani[5], and David Q. Matus[1¶*]

Affiliations:

1. Department of Biochemistry and Cell Biology, Stony Brook University, Stony Brook, NY 11794, United States.
2. Cold Spring Harbor Laboratory, Cold Spring Harbor, NY 11724, United States.
3. Howard Hughes Medical Institute, Department of Biology, Stanford University, Stanford, CA 94305, United States.
4. Science and Technology Research Program, Smithtown High School East, St. James, NY 11780, United States.
5. Departments of Biology and Cell Biology, University of Virginia, Charlottesville, VA 22904, United States.

***For correspondence:** tmkinney@unc.edu; david.matus@stonybrook.edu

Present address: [†]Department of Biology, University of North Carolina at Chapel Hill, Chapel Hill, NC 27599, United States; [‡]Touro College of Osteopathic Medicine, Middletown, NY 10940, United States; [§]Integra LifeSciences, Princeton, NJ 08540, United States; [#]Northeastern University, Boston, MA 02115, United States; [¶]Arcadia Science, Berkeley, CA 94704, United States.

Competing interest: David Q. Matus and Neha Somineni are paid employees of Arcadia Science and Integra LifeSciences, respectively.

Abstract

A growing body of evidence suggests that cell division and basement membrane invasion are mutually exclusive cellular behaviors. How cells switch between proliferative and invasive states is not well understood. Here, we investigated this dichotomy *in vivo* by examining two cell types that derive from equipotent progenitors, but exhibit distinct cell behaviors, in the developing *Caenorhabditis elegans* somatic gonad: the post-mitotic, invasive anchor cell and the neighboring proliferative, non-invasive ventral uterine (VU) cells. We report that the default invasive cellular state is suppressed in the VU cells through two distinct modes of regulation of the pro-invasive transcription factor NHR-67 (NR2E1/TLX). Levels of NHR-67 are important for discriminating between invasive and proliferative behavior, and *nhr-67* transcription is downregulated following post-translational degradation of its direct upstream regulator, HLH-2 (E/Daughterless) in VU cells. Residual NHR-67 protein is organized into discrete punctae in the nuclei of VU cells that are dynamic over the cell cycle and exhibit liquid-like properties. Strikingly, these NHR-67 punctae are not spatiotemporally associated with active transcription, but instead associate with homologs of the transcriptional co-repressor Groucho (UNC-37 and LSY-22), as well as the TCF/LEF homolog POP-1, likely mediated by a direct interaction between UNC-37 and the intrinsically disordered region of NHR-67. Further, perturbing UNC-37, LSY-22, or POP-1 results in ectopic invasive cells. We propose a model in which these proteins together form repressive condensates to suppress a default invasive state in non-invasive cells, which complements transcriptional regulation to add robustness to the proliferative-invasive cellular switch *in vivo*.

Introduction

Cellular proliferation and invasion are key aspects of development (reviewed in Medwig & Matus, 2017), and are also two of the defining hallmarks of cancer (reviewed in Hanahan and Weinberg, 2000). A growing body of evidence suggests that cell cycle progression and invasion through a basement membrane are mutually exclusive cellular

behaviors in both development and disease states (reviewed in Kohrman and Matus, 2017). Switching between invasive and proliferative phenotypes has been observed in melanoma and recently in breast cancer (Hoek et al., 2008; Mondal et al., 2021), but how these cell states are regulated in the context of development is not well understood. To investigate how this dichotomy in cellular behavior is controlled *in vivo*, we used *C. elegans*, leveraging its highly stereotypical development (Sulston and Horvitz, 1977), as well as its genetic and optical tractability. During development of the hermaphroditic reproductive system, the proximal granddaughters of the Z1 and Z4 somatic gonad progenitors, Z1.pp and Z4.aa, give rise to four cells that will adopt one of two cellular fates: a proliferative ventral uterine (VU) cell or the terminally differentiated, invasive anchor cell (AC) (Figure 1A) (Kimble and Hirsh, 1979). The distal cells of this competency group, Z1.ppa and Z4.aap, quickly lose their bipotentiality and become VU cells (Seydoux et al., 1990). In contrast, the proximal cells, Z1.ppp and Z4.aaa, undergo a stochastic Notch-mediated cell fate decision, giving rise to another VU cell and the post-mitotic AC (Figure 1A,B) (Greenwald et al., 1983; Seydoux and Greenwald, 1989). Following fate specification, the AC undergoes invasive differentiation and breaches the underlying basement membrane, connecting the uterus to the vulval epithelium to facilitate egg-laying (Figure 1B) (Sherwood and Sternberg, 2003).

Our previous work has shown that AC invasion is dependent on G_0 cell cycle arrest, which is coordinated by the pro-invasive transcription factor NHR-67 (NR2E1/TLX) (Figure 1–figure supplement 1A) (Matus et al., 2015). NHR-67 functions within a gene regulatory network comprised of four conserved transcription factors whose homologs have been implicated in several types of metastatic cancer (Liang and Wang, 2020; Milde-Langosch, 2005; Nelson et al., 2021; Wang and Baker, 2015). We previously reported that NHR-67 is regulated by a feed-forward loop formed by EGL-43 (Evi1) and HLH-2 (E/Daughterless), which functions largely in parallel to a cell cycle-independent subcircuit controlled by FOS-1 (Fos) (Figure 1–figure supplement 1A) (Medwig-Kinney et al., 2020). EGL-43, HLH-2, and NHR-67 are reiteratively used within the Z lineage of the somatic gonad, in that they also function to independently regulate LIN-12 (Notch) signaling during the initial AC/VU cell fate decision (Medwig-Kinney et al., 2020). Despite its role in lateral inhibition between Z1.ppp and Z4.aaa, expression of

94 LIN-12 is not absolutely required for VU cell fate (Sallee et al., 2015). Cell cycle state
95 also cannot explain the difference between AC and VU cell fates, as arresting VU cells
96 in G_0 through ectopic expression of CKI-1 (p21/p27) does not make them invasive
97 (Smith et al., 2022). Thus, the mechanisms responsible for maintaining AC and VU
98 cellular identities following initial cell fate specification remain unclear.
99 Maintenance of differentiated cell identity is essential for ensuring tissue integrity
100 during development and homeostasis, and the inability to restrict phenotypic plasticity is
101 now being recognized as an integral part of cancer pathogenesis (Hanahan, 2022). *In*
102 *vitro* studies have identified several factors that safeguard differentiated cell identity
103 (reviewed in Brumbaugh et al., 2019). Despite its largely autonomous modality of
104 development, *C. elegans* has emerged as an ideal model system to study cell fate
105 maintenance *in vivo*. There have been several reports of cell fate transformations that
106 occur naturally, including two epithelial-to-neural transdifferentiation events (Jarriault et
107 al., 2008; Riva et al., 2022), or following fate challenges (reviewed in Rothman and
108 Jarriault, 2019). In such contexts, several epigenetic factors, including chromatin
109 remodelers and histone chaperones, have been identified for their roles in restricting
110 cell fate reprogramming (Hajduskova et al., 2019; Kagias et al., 2012; Kolundzic et al.,
111 2018; Patel et al., 2012; Rahe and Hobert, 2019; Zuryn et al., 2014). However, in some
112 cases, ectopic expression of a specific transcription factor is sufficient to overcome
113 these barriers, as was first shown through pioneering work in mouse embryonic
114 fibroblasts (Davis et al., 1987). Indeed, there are several examples in *C. elegans* where
115 ectopic expression of single lineage-specific transcription factors induces cell fate
116 transformations (Fukushige and Krause, 2005; Gilleard and McGhee, 2001; Horner et
117 al., 1998; Jin et al., 1994; Kiefer et al., 2007; Quintin et al., 2001; Richard et al., 2011;
118 Riddle et al., 2013; Tursun et al., 2011; Zhu et al., 1998). Moreover, *C. elegans* uterine
119 tissue may be particularly amenable to fate transformations, as ectopic expression of a
120 single GATA transcription factor, ELT-7, is sufficient to induce transorganogenesis of
121 the somatic gonad into gut by reprogramming the mesodermally-derived tissue into
122 endoderm (Riddle et al., 2016). Valuable insights have been made into how the function
123 of fate-specifying transcription factors can be tuned through means such as
124 autoregulation and dynamic heterodimerization (Leyva-Díaz and Hobert, 2019; Sallee et

125 al., 2017). We are just beginning to understand how an additional layer of control over
126 transcriptional regulators can be achieved through the formation of higher order
127 associations (Boija et al., 2018; Lim and Levine, 2021).
128 Here, in our endeavor to understand how AC and VU cellular fates are
129 maintained, we identified two mechanisms of NHR-67 regulation that together modulate
130 the invasive-proliferative switch in *C. elegans*. We found that high levels of NHR-67
131 expression are sufficient to drive invasive differentiation and, accordingly, *nhr-67* is
132 transcriptionally downregulated in the non-invasive VU cells following the post-
133 translational degradation of its direct upstream regulator, HLH-2. Additionally, we
134 observed that remaining NHR-67 protein forms discrete punctae in the nuclei of non-
135 invasive cells that exhibit liquid-like properties including dynamic assembly, fusion, and
136 dissolution over cell cycle as well as rapid recovery kinetics after photobleaching. These
137 NHR-67 punctae colocalize *in vivo* with UNC-37 and LSY-22, homologs of the
138 transcriptional co-repressor Groucho, as well as with POP-1 (TCF/LEF), which are
139 mediated through a direct interaction between UNC-37 and the intrinsically disordered
140 C-terminal region of NHR-67. Through functional perturbations, we demonstrate that
141 UNC-37, LSY-22, and POP-1 normally function in repressing the default invasive state
142 in VU cells. We propose a model in which the interaction between NHR-67 and Groucho
143 coordinates formation of repressive condensates that, combined with transcriptional
144 downregulation of *nhr-67*, suppress invasive differentiation. This work provides new
145 insights into how repressive nuclear condensates may coordinate cellular behaviors *in*
146 *vivo* and highlights how transcription factors can exhibit duality in functions depending
147 on cellular context.
148
149 **<u>Results</u>**
150
151 **Levels of NHR-67 expression are important for distinguishing AC and VU cell**
152 **identity**
153 Despite arising from initially equipotent cells, the differentiated AC and VU cells
154 exhibit very distinct cellular behaviors. The AC terminally differentiates to invade the
155 underlying basement membrane while the VU cells remain proliferative, undergoing

156 several rounds of division before terminally differentiating into the pi (π) and rho (ρ) cells
157 that function in uterine-vulval attachment. One potential explanation for this difference in
158 cell behavior is asymmetric expression of pro-invasive transcription factors. To
159 investigate this possibility, we examined endogenous expression levels of four
160 transcription factors that function in the gene regulatory network coordinating AC
161 invasion (EGL-43, FOS-1, HLH-2, and NHR-67) using previously generated GFP-
162 tagged alleles (Medwig-Kinney et al., 2020). While FOS-1 levels of expression in the AC
163 are nearly twice that of the VU cells (Figure 1–figure supplement 1B,C), FOS-1 has no
164 identified role in regulating cell cycle in the AC so we did not pursue this protein further
165 (Medwig-Kinney et al., 2021). EGL-43 also did not appear to be a promising candidate,
166 as it is expressed in both cell types at comparable levels, with VU cells exhibiting
167 approximately 89% of AC expression (Figure 1–figure supplement 1B,C). In contrast,
168 HLH-2 exhibits significant asymmetry in expression, as VU cells express merely 17% of
169 HLH-2 levels observed in the AC on average (Figure 1C,D). Previous studies have
170 shown that post-translational, dimerization-driven degradation of HLH-2 is responsible
171 for its downregulation in the VU cells (Benavidez et al., 2022; Karp and Greenwald,
172 2003; Sallee and Greenwald, 2015). Endogenously tagged NHR-67::GFP exhibits a
173 similar pattern of expression with over three-fold enrichment in the AC, consistent with
174 prior observations of transgenic reporters (Figure 1C,D) (Verghese et al., 2011). Given
175 the known role of NHR-67 in regulating cell cycle arrest and invasion, we hypothesized
176 that its differential expression between the AC and VU cells could potentially be
177 contributing to their distinct cellular behaviors.
178 To assess if NHR-67 plays a role in regulating uterine cell identities, we
179 manipulated its expression levels. We found that strong depletion of NHR-67 through
180 RNA interference (RNAi) treatment results in ACs adopting VU-like characteristics.
181 During AC/VU cell fate specification, LIN-12/Notch normally becomes restricted to the
182 VU cells while the Delta-like ligand LAG-2 (visualized by LAG-
183 2::P2A::H2B::mTurquoise2 (Medwig-Kinney et al., 2022)) accumulates in the AC
184 (Wilkinson et al., 1994). Here, we observe that NHR-67 deficient ACs not only
185 proliferated and failed to invade, as reported previously (Matus et al., 2015), but also
186 ectopically expressed membrane-localized Notch (visualized by LIN-12::mNeonGreen

187 (Pani et al., 2022)) (Figure 1E). Notably, NHR-67-deficient ACs expressed both LIN-12
188 and LAG-2, potentially indicating an intermediate state between AC and VU cell fate
189 (Figure 1E). Next, we ectopically expressed NHR-67 ubiquitously using a heat shock
190 inducible transgene (*hsp*::NHR-67::2x-BFP) (Medwig-Kinney et al., 2020). Intriguingly,
191 we observed that ectopic expression of NHR-67 following initial AC/VU specification
192 resulted in the presence of multiple invasive ACs at a low penetrance (approximately
193 5%, n > 50), denoted by ectopic expression of an AC marker (*cdh-*
194 *3p*::mCherry::moeABD) and expansion of the basement membrane gap (Figure 1F).
195 Since it has been previously demonstrated that proliferative ACs cannot invade (Matus
196 et al., 2015), we concluded that these invasive ectopic ACs most likely arose from fate
197 conversion of neighboring VU cells. Taken together, these pieces of evidence suggest
198 that high and low levels of NHR-67 expression correlate to properties of AC and VU cell
199 identities, respectively (Figure 1G).
200
201 **NHR-67 is enriched in the AC through direct transcriptional regulation by HLH-2**
202 Next, we investigated how NHR-67 expression levels become asymmetric
203 between the AC and VU cells. We and others have previously shown that HLH-2
204 positively regulates NHR-67 expression in the context of the AC (Figure 1–figure
205 supplement 1A) (Bodofsky et al., 2018; Medwig-Kinney et al., 2020). If this regulatory
206 interaction exists in the context of the VU cells as well, it could explain why the relative
207 expression pattern of NHR-67 in the AC and VU cells mirrors that of HLH-2. In support
208 of this hypothesis, we found that initial onset of HLH-2, which has shown to be
209 asymmetric in Z1.pp and Z4.aa (Attner et al., 2019), correlates to that of NHR-67 onset
210 (Figure 2–figure supplement 1A). To test whether HLH-2 degradation is responsible for
211 NHR-67 downregulation in the VU, we drove ectopic expression of HLH-2 using a
212 transgene under the control of a heat shock inducible promoter (*hsp*::HLH-2::2x-BFP)
213 (Medwig-Kinney et al., 2020). We observed that ectopic expression of HLH-2 resulted in
214 elevated NHR-67 expression in VU cells (43% increase; n > 30) (Figure 2A,B). To
215 control against potential dimerization-driven degradation of HLH-2 in the VU cells, which
216 the heat shock inducible transgene would still be susceptible to, we disrupted UBA-1, an
217 E1 ubiquitin-activating enzyme that has recently been shown to be necessary for HLH-2

218 degradation in VU cells (Benavidez et al., 2022). Following perturbation of UBA-1
219 through RNAi treatment, HLH-2 expression in the VU cells increased more than four-
220 fold and NHR-67 expression increased by nearly 60% compared to the empty vector
221 control (Figure 2–figure supplement 1B-D). Both experiments suggest that *nhr-67*
222 expression in the VU cells is at least partially regulated by levels of HLH-2.
223 It has previously been proposed that the interaction between HLH-2 and *nhr*-67
224 is direct. This is based on the identification of E binding motifs within a 276 bp region of
225 the *nhr-67* promoter that is required for NHR-67 expression in the uterine tissue and
226 encompasses the location of several hypomorphic mutations (*pf2*, *pf88*, *pf159*) (Figure
227 2C) (Bodofsky et al., 2018; Verghese et al., 2011). We confirmed this interaction
228 through a yeast one-hybrid assay after generating a bait strain containing this *nhr-67*
229 promoter region and pairing it with an HLH-2 Gal4-AD prey plasmid from an existing
230 yeast one-hybrid library (Reece-Hoyes et al., 2005). Yeast growth on the selective SC-
231 HIS-TRP plates containing the competitive inhibitor 3-aminotriazole (3-AT)
232 demonstrated that HLH-2 does indeed bind directly to this 276 bp region of the *nhr-67*
233 promoter (Figure 2D). Together, these results suggest that direct transcriptional
234 regulation of *nhr-67* by HLH-2 contributes to the asymmetry in NHR-67 expression
235 between the AC and VU cells.
236
237 **NHR-67 forms dynamic punctae in VU cell nuclei that exhibit liquid properties**
238 Upon closer examination of GFP-tagged NHR-67, it became evident that the AC
239 and VU cells not only exhibit differences in overall NHR-67 levels, but also in
240 localization of the protein. While NHR-67 localization is fairly uniform throughout the AC
241 nucleus (excluding the nucleolus), we often observed discrete punctae throughout the
242 nuclei of VU cells (Figure 3A,B). These punctae were observed with NHR-67
243 endogenously tagged with several different fluorescent proteins, including GFP,
244 mNeonGreen, mScarlet-I, and TagRFP-T (Figure 3–figure supplement 1A,B).
245 Furthermore, by utilizing a live-cell imaging approach, we would not expect to encounter
246 artificial puncta formation that can result from tissue fixation methods (Irgen-Gioro et al.,
247 2022). Thus, NHR-67 puncta formation in the VU cells does not appear to be an artifact
248 of the fluorophore or sample preparation.

249 To characterize dynamics of these punctae during interphase states of the cell
250 cycle, we paired GFP-tagged NHR-67 with a CDK activity sensor. The CDK activity
251 sensor is comprised of a fragment of DNA Helicase B (DHB) fused to a fluorophore (2x-
252 mKate2), expressed under a ubiquitous promoter (Figure 3C) (Adikes et al., 2020). DHB
253 contains a strong nuclear localization signal (NLS), flanked by four serine sites, as well
254 as a weaker nuclear export signal (NES). As CDK activity increases over the cell cycle,
255 the CDK sensor is translocated from the nucleus to the cytoplasm, allowing for
256 correlation of its relative subcellular localization to cell cycle state (Figure 3C) (Adikes et
257 al., 2020; Spencer et al., 2013). Time-lapse microscopy revealed that the number of
258 NHR-67 punctae was dynamic over the course of the cell cycle, with punctae first
259 appearing shortly after mitotic exit in the G1 phase, and then reducing in number to two
260 large punctae prior to nuclear envelope breakdown before disappearing (Figure 3D,E).
261 We collected additional recordings with finer time resolution and captured fusion, or
262 condensation, of punctae prior to their dissolution (representative of 6 biological
263 replicates) (Figure 3F). These punctae also exhibit relatively rapid diffusion kinetics, as
264 observed by fluorescence recovery following photobleaching ($t_{1/2}$ = 46 seconds; n = 8)
265 at a rate within the same order of magnitude as P granule proteins PGL-1 and PGL-3
266 (Figure 3G,H) (Putnam et al., 2019). These properties of NHR-67 punctae are
267 consistent with those observed with proteins that form nuclear condensates.
268
269 **Groucho homologs UNC-37 and LSY-22 associate with NHR-67 punctae and**
270 **contribute to VU cell fate**
271 In a first step towards defining the role of putative NHR-67 condensates, we
272 tested the extent to which NHR-67 punctae colocalized with homologs of other proteins
273 known to form nuclear condensates by pairing GFP- and mScarlet-I-tagged NHR-67
274 with other endogenously tagged alleles. As NHR-67 is a transcription factor, it is
275 reasonable to speculate that its punctae may represent clustering around sites of active
276 transcription, which would be consistent with data showing RNA Polymerase II and the
277 Mediator complex can associate with transcription factors through phase separation
278 (Cho et al., 2018). To test this hypothesis, we co-visualized NHR-67 with a GFP-tagged
279 allele of *ama-1*, the amanitin-binding subunit of RNA polymerase II (Hills-Muckey et al.,

280 2021) and failed to observe significant colocalization between NHR-67 and AMA-1
281 punctae (Manders' overlap coefficient, M = 0.066) compared to negative controls where
282 a single channel was compared to its 90-degree rotation (M = 0.108) (Figure 4A,B).
283 Another possibility considered is that NHR-67 localization is indicative of chromatin
284 organization, as heterochromatin has been shown to be compartmentalized in the
285 nucleus through phase separation (Larson et al., 2017; Strom et al., 2017). However,
286 we did not observe significant colocalization of NHR-67 with the endogenously tagged
287 HP1 heterochromatin proteins (Patel and Hobert, 2017) HPL-1 (M = 0.076) or HPL-2 (M
288 = 0.083) (Figure 4A,B). Recent work in *Ciona* embryos has shown that the
289 transcriptional co-repressor Groucho forms repressive condensates in nuclei through
290 phase separation (Treen et al., 2021). The *C. elegans* genome encodes one Groucho
291 homolog, UNC-37, as well as a Groucho-like protein, LSY-22. To examine their
292 localization compared to NHR-67, we tagged LSY-22 with TagRFP-T (Figure 4–figure
293 supplement 1) and acquired a mNeonGreen-tagged allele of *unc-37* (Ma et al., 2021).
294 Strikingly, we observed significant colocalization of NHR-67 punctae with both LSY-22
295 (M = 0.686) and UNC-37 (M = 0.741), comparable to colocalization measures in
296 heterozygous NHR-67::mScarlet-I/NHR-67::GFP animals (M = 0.651), which were used
297 as positive controls (Figure 4A,B). This evidence suggests that NHR-67 punctae do not
298 localize to sites of active transcription or chromatin compaction, but instead associate
299 with transcriptional co-repressors.
300 Since the AC is the default state of the AC/VU cell fate decision (Seydoux and
301 Greenwald, 1989), we hypothesized that the punctae including NHR-67, UNC-37, and
302 LSY-22 may function in repressing invasive differentiation. To test this hypothesis, we
303 depleted UNC-37 and LSY-22 utilizing the auxin inducible degron (AID) protein
304 degradation system, in which a protein of interest is tagged with an AID that is
305 recognized by TIR1 in the presence of auxin and ubiquitinated by the SCF E3 ubiquitin
306 ligase complex (Figure 4C) (Martinez et al., 2020; Zhang et al., 2015). We re-tagged
307 LSY-22 with mNeonGreen::AID (Figure 4–figure supplement 1) and acquired a
308 BFP::AID-tagged allele of *unc-37* (Kurashina et al., 2021). Each AID-tagged allele was
309 paired with a transgene encoding *Arabidopsis thaliana* TIR1 ($_{At}$TIR1) that was co-
310 expressed with a nuclear-localized mCherry::HIS-11. Following auxin treatment, we

311 observed ectopic expression of an AC marker (*cdh-3p*::mCherry::moeABD) in 28% of
312 LSY-22::AID animals and 59% of UNC-37::AID animals (n = 64 for both) (Figure 4D).
313 These results are consistent with phenotypes we observed in genetic backgrounds with
314 *unc-37* hypomorphic (*unc-37(e262wd26)*) and null (*unc-37(wd17wd22)*) mutant alleles
315 (Figure 4–figure supplement 2). It is likely that dual depletion of UNC-37 and LSY-22
316 would result in a higher penetrance of ectopic ACs given their partial redundancy in
317 function (Flowers et al., 2010), but animals possessing both AID-tagged alleles were not
318 viable when paired with the $_{At}$TIR1 transgene.
319
320 **TCF/LEF homolog POP-1 associates with NHR-67/Groucho punctae and is**
321 **necessary for VU cell maintenance post-specification**
322 While UNC-37/LSY-22 colocalization with NHR-67 punctae and ectopic AC
323 phenotypes are consistent with roles in coordinating AC and VU cell fates, both genes
324 are broadly expressed and exhibit comparable levels (<10% difference) between the
325 two cell types (Figure 5A,C; Figure 5–figure supplement 1A,B). Therefore, we
326 hypothesized that another factor must be involved that confers VU cell specificity to
327 Groucho-mediated repression of invasiveness. It had previously been reported that the
328 sole TCF/LEF homolog in *C. elegans*, POP-1, forms a repressive complex with UNC-37
329 in the early embryo to restrict expression of the endoderm-determining gene, END-1
330 (Calvo et al., 2001). Additionally, POP-1 has a known role in development of the
331 somatic gonad, as perturbing its function results in ectopic ACs (Siegfried and Kimble,
332 2002). Examination of an eGFP-tagged *pop-1* allele (van der Horst et al., 2019),
333 showed significant enrichment in the VU cells (>20%) compared to the AC (Figure 5B,C;
334 Figure 5–figure supplement 1A,B). We also observed that POP-1 forms punctae in the
335 nuclei of VU cells, which had previously been observed during interphase in non-Wnt
336 signaled embryonic cells (Maduro et al., 2002). We found that these POP-1 punctae
337 colocalize with NHR-67 (M = 0.547), although to a lesser degree than UNC-37 and LSY-
338 22, likely because the strong POP-1 fluorescence outside of punctae made them more
339 difficult to segment (Figure 5D,E). Additionally, *nhr-67(RNAi)* treatment resulted in a
340 significant increase in AC expression of eGFP::POP-1 compared to empty vector
341 controls (225%, n > 30), a pattern we observed following depletion of other transcription

342 factors (Medwig-Kinney et al., 2020) and chromatin modifiers (Smith et al., 2022)
343 required for AC arrest and invasion (Figure 5F,G; Figure 5–figure supplement 2A,B).
344 This negative regulation of POP-1 by NHR-67 may explain why the proteins have
345 opposite patterns of enrichment.

346 It has previously been suggested that POP-1 may be functioning as an activator
347 in the VU precursors Z1.ppa and Z4.aap based on the relative expression of a POP-1
348 transgene (Sallee et al., 2015). This view is largely dependent on the notion that high
349 levels of POP-1 correlate to repressive function and low levels are conducive for
350 activator roles (Shetty et al., 2005). In contrast, we did not find evidence of
351 transcriptional activation by POP-1 in the AC/VU precursors nor their differentiated
352 descendants using an established POPTOP (POP-1 and TCF optimal promoter)
353 reporter, which contains seven copies of POP-1/TCF binding sites and the *pes-10*
354 minimal promoter (Figure 5F; Figure 5–figure supplement 3A,B) (Green et al., 2008).
355 The growing consensus regarding the Wnt/β-catenin asymmetry pathway is that relative
356 levels of POP-1 and β-catenin are more important than absolute protein levels of POP-1
357 (Phillips and Kimble, 2009). Our proposed model of POP-1 acting as a repressor in the
358 proximal gonad is consistent with the finding that SYS-1 (β-catenin) expression is
359 restricted to the distal gonad early in somatic gonad development and is not detectable
360 in the AC or VU cells (Figure 5–figure supplement 3C) (Phillips et al., 2007; Sallee et al.,
361 2015). It is also supported by recent evidence suggesting that UNC-37/LSY-22 mutant
362 alleles phenocopy *pop-1* knockdown, which produces ectopic distal tip cells (Bekas and
363 Phillips, 2022).

364 One aspect that makes studying the repressive role of POP-1 in cell fate
365 maintenance challenging is that its activator function is required for distal cell fate
366 specification in the somatic gonad earlier in development. Loss of either POP-1 and
367 SYS-1 results in a Sys (symmetrical sister cell) phenotype, where all somatic gonad
368 cells adopt the default proximal fate and thereby give rise to ectopic ACs (Siegfried and
369 Kimble, 2002; Siegfried et al., 2004). This likely occluded previous identification of the
370 repressive role of POP-1 in maintaining VU cell fates. To achieve temporal control over
371 POP-1 expression to tease apart its two opposing roles, we inserted an AID tag into the
372 N-terminus of the *pop-1* locus; however, this resulted in gonadal defects even in the

absence of both TIR1 and auxin. Instead, using tools at hand, we paired eGFP-tagged POP-1 with a uterine-specific anti-GFP nanobody (Smith et al., 2022; Wang et al., 2017). The anti-GFP nanobody is fused to ZIF-1 and serves as an adapter, recognizing GFP-tagged proteins and promoting their ubiquitination by the Cullin2-based E3 ubiquitin ligase, which ultimately targets them for degradation via the proteasome (Figure 6–figure supplement 1A) (Wang et al., 2017). This anti-GFP nanobody, visualized by nuclear expression of mCherry, was not detectable prior to or even shortly after the AC/VU cell fate decision, which allowed us to bypass disruption of initial cell specification (Figure 6–figure supplement 1B). While this method only produced a mild knockdown of POP-1 in the VU cells, we still observed the ectopic AC phenotype at low penetrance (7%, n = 60) (Figure 6–figure supplement 1C). To achieve stronger depletion, we used RNAi for further POP-1 perturbations.

To interrogate the phenotypic consequences of POP-1 perturbation, we utilized a strain expressing two markers of AC fate (*cdh-3p*::mCherry::moeABD and LAG-2::P2A::H2B::mTurquoise2). Following treatment with *pop-1(RNAi)*, we observed several animals with two or more bright *cdh-3/lag-2*+ ACs, consistent with known phenotypes caused by cell fate misspecification in the somatic gonad (17%, n = 30) (Figure 6A). We also observed animals with invasive cells that express AC markers at inconsistent levels (53%, n = 30), suggesting that the cells did not adopt AC fate at the same time (Figure 6A). To test whether the subset of dim *cdh-3/lag-2*+ ACs are the result of VU-to-AC cell fate conversion, we visualized AC and VU fates simultaneously using the AC markers previously described along with an mNeonGreen-tagged allele of *lag-1* (CSL), a protein downstream of Notch signaling whose expression becomes restricted to the VU cells following AC/VU cell fate specification. Following treatment with *pop-1(RNAi)*, we found that a subset of ectopic ACs co-express AC markers and LAG-1, likely indicating an intermediate state between the two cell types (Figure 6–figure supplement 2). To visualize this process live, we used time-lapse microscopy and were able to capture ectopic ACs gradually upregulating LAG-2 (+51%, n = 3) and downregulating LAG-1 (-16%, n = 3) over time (Figure 6B,C), consistent with VU-to-AC cell fate conversion.

404 **IDR of NHR-67 facilitates protein-protein interaction with UNC-37**

405 Given that UNC-37, LSY-22, and POP-1 phenocopy each other with respect to
406 AC/VU fates and all three colocalize with NHR-67 punctae, we next sought to further
407 characterize the interactions among these proteins. Previous work has either directly
408 identified or predicted protein-protein interactions among POP-1, UNC-37, and LSY-22
409 (Boxem et al., 2008; Calvo et al., 2001; Flowers et al., 2010; Reece-Hoyes et al., 2005;
410 Simonis et al., 2009; Zhong and Sternberg, 2006). Using a yeast two-hybrid assay with
411 UNC-37 Gal4-AD prey, we confirmed that UNC-37 directly interacts with both POP-1
412 and LSY-22 after observing yeast growth on the selective SC-HIS-TRP-LEU plates
413 containing 3-AT (Figure 7–figure supplement 1). Using the same technique, we found
414 that NHR-67 binds directly to UNC-37, as previously predicted (Li et al., 2004; Simonis
415 et al., 2009), but found no evidence of it directly interacting with LSY-22 or POP-1
416 (Figure 7–figure supplement 1).

417 To further characterize the protein-protein interaction between NHR-67 and
418 UNC-37, we assessed the protein structure of NHR-67 using AlphaFold, an artificial
419 intelligence-based protein structure prediction tool (Jumper et al., 2021; Varadi et al.,
420 2022), and PONDR, a predictor of intrinsic disorder (Peng and Zhang, 2006). Both
421 identify an intrinsically disordered region (IDR) at the C-terminus of NHR-67 (Figure
422 7A,B). IDRs are low complexity domains that lack fixed three-dimensional structure and
423 have been shown to support dynamic protein-protein interactions (Chong et al., 2018).
424 To determine if the IDR of NHR-67 is important for facilitating its interaction with UNC-
425 37, we repeated the yeast two-hybrid experiment using UNC-37 Gal4-AD prey, pairing it
426 with different fragments of the NHR-67 protein: full-length, without its IDR (ΔIDR), and
427 its IDR alone (Figure 7C,D). Yeast growth on the selective SC-HIS-TRP-LEU plates
428 containing the competitive inhibitor 3-aminotriazole (3-AT) demonstrates that the 108
429 amino acid IDR sequence of NHR-67 is necessary and sufficient to bind with UNC-37
430 (Figure 7C,D).

431 Thus, our current model supported by the data shown here proposes that NHR-
432 67 levels are controlled through two distinct mechanisms. First, transcription of *nhr-67* is
433 directly regulated by HLH-2, resulting in enrichment in the AC compared to the VU.
434 Second, in the AC, where NHR-67 levels are high and POP-1 is repressed, NHR-67 is

free to activate genes promoting invasive differentiation. In the VU cells, where NHR-67 levels are low and POP-1 levels are high, POP-1 assembles with LSY-22, UNC-37, and NHR-67 to repress NHR-67 targets (Figure 7E). It is possible that POP-1 negatively regulates NHR-67 at the transcriptional level as well, as the *nhr-67* promoter contains 7 putative TCF binding sites (Zacharias et al., 2015). Taken together, our findings reveal a dual mechanism for repressing NHR-67 activity in the proliferative VU cells, maintaining their proliferative fates while suppressing the acquisition of an invasive phenotype.

Discussion

In summary, here we provide evidence that activity of the pro-invasive transcription factor, NHR-67, is simultaneously regulated by two distinct processes, which together modulate the proliferative-invasive switch in *C. elegans*. We show that NHR-67 is a potent fate-specifying transcription factor, in that its expression is sufficient for invasive differentiation of ACs in the somatic gonad. This could explain why NHR-67 needs to be post-translationally sequestered in addition to being transcriptionally downregulated in non-invasive cells to fully suppress its function in activating the pro-invasive program. We also discovered that NHR-67 forms nuclear foci in non-invasive cells, which exhibit liquid-like properties, indicated by observations of their condensation, dissolution, and relatively rapid recovery from photobleaching, similar to what has been described with P granules (Brangwynne et al., 2009). These NHR-67 punctae associate with Groucho homologs, UNC-37 and LSY-22, through a direct protein-protein interaction with UNC-37 mediated by the C-terminal IDR of NHR-67. We postulate that this association leads to formation of repressive condensates, as has recently been described in *Ciona* embryos (Treen et al., 2021). Furthermore, Groucho-mediated repression of the default invasive state appears to be dependent on expression of the TCF/LEF homologs POP-1, which clarifies our understanding of the dual roles this protein plays during development of the somatic gonad. It is also interesting to note that the dynamic punctae formed by POP-1 in non-Wnt signaled cells was first described 20 years ago (Maduro et al., 2002), but their function are only now being appreciated in light of recent advances in our understanding of the formation of

466 higher order associations in the nucleus.

467 With regard to phase separation in the nucleus, most research has been through
468 the lens of transcriptional activation through RNA Polymerase II and the mediator
469 complex (Boija et al., 2018; Cho et al., 2018; Sabari et al., 2018) or repression through
470 condensate formation with HP1 heterochromatin proteins (Larson et al., 2017; Strom et
471 al., 2017). Rather than functioning through either of these established mechanisms, we
472 have identified here the second observed case of Groucho-mediated repressive
473 condensates (Treen et al., 2021), which suggests that Groucho proteins may have
474 evolutionarily conserved roles in repressing transcription through the formation of
475 nuclear condensates within the Metazoa. Further, we demonstrate how this repressive
476 mechanism can control cell biology *in vivo* using endogenously tagged alleles and a
477 clear cell biological read-out of fate and function: invasion versus proliferation.

478 Still, as this is one of the first studies into the role of repressive condensates *in*
479 *vivo*, there is much left to learn. For example, it is unknown whether DNA binding is
480 necessary for nuclear puncta formation. The interaction between UNC-37 and NHR-67
481 does not appear to depend on DNA binding, as the C-terminal IDR region of NHR-67
482 (excluding its zinc finger domains) was sufficient for binding with UNC-37 *in vitro*, but it
483 is possible that DNA binding is needed for oligomerization *in vivo*. Furthermore, it
484 remains unclear if suppression of invasive differentiation is achieved by simply
485 sequestering the pro-invasive transcription factor NHR-67 away from its transcriptional
486 targets or through direct repression of transcription. If the latter, another question that
487 arises is how the repressive complex gets recruited to specific genomic sites, since
488 POP-1 and NHR-67 are both capable of binding to DNA, and whether repression is
489 achieved through competition with transcriptional activators or recruitment of histone
490 deacetylases. Direct targets of NHR-67 have not yet been discovered, which makes it
491 difficult to investigate this specific aspect of the repressive mechanism at present. We
492 see this as a promising avenue of future study as technologies advance, allowing for
493 transcriptional profiling and target identification in specific tissues or cells (Gómez-
494 Saldivar et al., 2020; Katsanos and Barkoulas, 2022).

495 In this work, we have also identified several perturbations (i.e., increasing levels
496 of NHR-67, decreasing levels of UNC-37/LSY-22) that result in incompletely penetrant

497 transdifferentiation phenotypes and/or intermediate cell fates. We foresee these being
498 ideal cell fate challenge backgrounds in which to perform screens to identify regulators
499 of cellular plasticity, as has been done in other contexts (Rahe and Hobert, 2019).
500 Additionally, these induced fate transformations can be paired with tools to visualize and
501 manipulate cell cycle (Adikes et al., 2020) to determine if any cell cycle state is
502 particularly permissive for cell fate plasticity. While G1 arrest has been shown to
503 enhance conversion of human fibroblasts to dopaminergic neurons (Jiang et al., 2015),
504 mitosis is required for the natural K-to-DVB transdifferentiation event in *C. elegans* (Riva
505 et al., 2022). As control of proliferation and invasion, as well as maintenance of
506 differentiated cellular identities, are important for both homeostatic and disease states, it
507 is our hope that this work will shed light on how cells switch between these states in the
508 context of cancer growth and metastasis.
509

510 **Materials and methods**

511

512 **Key resources table**

Reagent type (species) or resource	Designation	Source or reference	Identifiers	Additional information
Strain, strain background (*C. elegans*)	DQM335	Medwig-Kinney et al. (2020)		*egl-43*(*bmd88*[*egl-43p*::EGL-43::loxP::GFP::EGL-43]) II; *qyIs225*[*cdh-3p*::mCherry::moeABD] V; *qyIs7*[laminin::GFP] X.
Strain, strain background (*C. elegans*)	DQM350	Medwig-Kinney et al. (2020)		*hlh-2*(*bmd90*[*hlh-2p*::loxP::GFP::HLH-2]) I; *qyIs225*[*cdh-3p*::mCherry::moeABD] V; *qyIs7*[laminin::GFP] X.
Strain, strain background (*C. elegans*)	DQM354	This paper		*nhr-67*(*syb509*[*nhr-67p*::NHR-67::GFP]) IV; *bmd66*[loxP::*egl-43p*::GFP-nanobody::P2A::HIS-58::mCherry] I; *qyIs225*[*cdh-3p*::mCherry::moeABD] V; *qyIs7*[laminin::GFP] X.
Strain, strain background (*C. elegans*)	DQM368	Medwig-Kinney et al. (2020)		*nhr-67*(*syb509*[*nhr-67p*::NHR-67::GFP]) IV; *qyIs225*[*cdh-3p*::mCherry::moeABD] V; *qyIs7*[laminin::GFP] X.
Strain, strain background (*C. elegans*)	DQM444	Medwig-Kinney et al. (2020)		*bmd121*[*hsp::*NHR-67::2x-BFP] I; *qyIs227*[*cdh-3p*::mCherry::moeABD] I; *qyIs7*[laminin::GFP] X.

Strain, strain background (*C. elegans*)	DQM515	Medwig-Kinney et al. (2020)		*fos-1*(*bmd138*[*fos-1p*::loxP::GFP::FOS-1]) V; *qyIs227*[*cdh-3p*::mCherry::moeABD] I; *qyIs7*[laminin::GFP] X.
Strain, strain background (*C. elegans*)	DQM704	Medwig-Kinney et al. (2021)		*nhr-67*(*bmd212*[*nhr-67p*::NHR-67::TagRFP-T::AID]) IV; *hlh-2*(*bmd90*[*hlh-2p*::LoxP::GFP::HLH-2]) I.
Strain, strain background (*C. elegans*)	DQM800	This paper		*pop-1*(*he335*[*pop-1p*::eGFP::loxP::POP-1]) I; *syIs187*[*pes-10*::7XTCF-mCherry-let-858(3'UTR) + unc-119(+)].
Strain, strain background (*C. elegans*)	DQM811	This paper		*qyIs227*[*cdh-3p*::mCherry::moeABD] I; *lam-2*(*qy20*[*lam-2p*::LAM-2::mNeonGreen]) X; *lag-2*(*bmd202*[*lag-2p*::LAG-2::P2A::H2B::mTurquoise2^lox511^2xHA]) V.
Strain, strain background (*C. elegans*)	DQM853	This paper		*hlh-2*(*bmd90*[*hlh-2p*::loxP::GFP::HLH-2]) I; *stIs11476*[*nhr-67p*::NHR-67::H1-wCherry + *unc-119(+)*].
Strain, strain background (*C. elegans*)	DQM957	This paper		*csh128*[*rpl-28p*::TIR1::T2A::mCherry::his-11)] II; *qyIs225*[*cdh-3p*:: mCherry::moeABD] V; *qyIs7*[laminin::GFP] X.
Strain, strain background (*C. elegans*)	DQM958	This paper		*csh140*[*rpl-28p*::TIR1(F79G)::T2A::mCherry::his-11)] II; *qyIs225*[*cdh-3p*:: mCherry::moeABD] V; *qyIs7*[laminin::GFP] X.
Strain, strain background (*C. elegans*)	DQM971	This paper		*pop-1*(*he335*[*pop-1p*::eGFP::loxP::POP-1]) I; *qyIs225*[*cdh-3p*::mCherry::moeABD] V; *qyIs7*[laminin::GFP] X.
Strain, strain background (*C. elegans*)	DQM989	This paper		*unc-37*(*devKi218*[*unc-37p*::mNeonGreen::UNC-37]) I; *qyIs225*[*cdh-3p*::mCherry::moeABD] V; *qyIs7*[laminin::GFP] X.
Strain, strain background (*C. elegans*)	DQM990	This paper		*unc-37(e262wd26)* I; *qyIs225*[*cdh-3p*::mCherry::moeABD] V; *qyIs7*[laminin::GFP] X.
Strain, strain background (*C. elegans*)	DQM1003	This paper		*nhr-67*(*syb509*[*nhr-67p*::NHR-67::GFP]) IV; *bmd168*[*rps-27p*::DHB::2x-mKate2] II.
Strain, strain background (*C. elegans*)	DQM1006	This paper		*lsy-22*(*bmd275*[*lsy-22p*::loxP::mNeonGreen::AID::LSY-22]) I; *qyIs225*[*cdh-3p*::mCherry::moeABD] V; *qyIs7*[laminin::GFP] X.
Strain, strain background (*C. elegans*)	DQM1008	This paper		*pop-1*(*he335*[*pop-1p*::eGFP::loxP::POP-1]) I; *bmd277*[loxP::*egl-43p*::GFP-nanobody::P2A::HIS-58::mCherry] I;

				qyIs225[*cdh-3p*::mCherry::moeABD] V; *qyIs7*[laminin::GFP] X.
Strain, strain background (*C. elegans*)	DQM1009	This paper		*unc-37*(*devKi218*[*unc-37p*::mNeonGreen::UNC-37]) I; *nhr-67*(*wy1633*[*nhr-67p*::NHR-67::mScarlet-I::AID*::3xFLAG]) IV.
Strain, strain background (*C. elegans*)	DQM1010	This paper		*hpl-2*(*ot860*[*hpl-2p*::HPL-2::mKate2::HPL-2]) III; *nhr-67*(syb509[*nhr-67p*::NHR-67::GFP]) IV.
Strain, strain background (*C. elegans*)	DQM1011	This paper		*hpl-1*(*ot841*[*hpl-1p*::HPL-1::mKate2::HPL-1]) X; *nhr-67*(*syb509*[*nhr-67p*::NHR-67::GFP]) IV.
Strain, strain background (*C. elegans*)	DQM1012	This paper		*lsy-22*(*bmd214*[*lsy-22p*::lox2272::TagRFP-T::AID::LSY-22]) I; *nhr-67*(*syb509*[*nhr-67p*::NHR-67::GFP]) IV.
Strain, strain background (*C. elegans*)	DQM1013	This paper		*pop-1*(*he335*[*pop-1p*::eGFP::loxP::POP-1]) I; *nhr-67*(*syb509*[*nhr-67p*::NHR-67::GFP]) IV.
Strain, strain background (*C. elegans*)	DQM1014	This paper		*unc-37*(*wd17wd22*)/hT2[*bli-4*(*e937*) *let-?*(*q782*) *qIs48*] (I, III); *qyIs225*[*cdh-3p*::mCherry::moeABD] V; *qyIs7*[laminin::GFP] X.
Strain, strain background (*C. elegans*)	DQM1017	This paper		*ama-1*(*ers49*[*ama-1p*::AMA-1::AID::GFP]) IV; *nhr-67*(*wy1633*[*nhr-67p*::NHR-67::mScarlet-I::AID*::3xFLAG]) IV.
Strain, strain background (*C. elegans*)	DQM1051	This paper		*lin-12(ljf31*[*lin-12*::mNeonGreen[C1]^loxP^3xFlag]) III; *lag-2*(*bmd202*[*lag-2p::*LAG-2::P2A::H2B::mTurquoise2^lox511^2xHA]) V.
Strain, strain background (*C. elegans*)	DQM1081	This paper		*bmd168*[*rps-27p*::DHB::2x-mKate2] II; *egl-13*(*devKi199*[*egl-13p*::EGL-13::mNeonGreen]) X; *lag-2*(*bmd202*[*lag-2p*::LAG-2::P2A::H2B::mTurquoise2]) V.
Strain, strain background (*C. elegans*)	DQM1101	This paper		*lsy-22*(*bmd275*[*lsy-22p*::^loxP^mNeonGreen::AID::LSY-22]) I; *csh128*[*rpl-28p*::TIR1::P2A::mCherry::his-11)] II; *qyIs225*[*cdh-3p*:: mCherry::moeABD] V; *qyIs7*[laminin::GFP] X.
Strain, strain background (*C. elegans*)	DQM1115	This paper		*unc-37*(*miz36*[*unc-37p*::UNC-37::AID::BFP]) I; *csh128*[*rpl-28p*::TIR1::P2A::mCherry::his-11)] II; *qyIs225*[*cdh-3p*:: mCherry::moeABD] V; *qyIs7*[laminin::GFP] X.

Strain, strain background (*C. elegans*)	DQM1127	This paper		*nhr-67*(*syb509*[*nhr-67p*::NHR-67::GFP]) IV; *stIs11476*[*nhr-67p*::NHR-67::H1-wCherry + unc-119(+)].
Strain, strain background (*C. elegans*)	DQM1129	This paper		*bmd143*[*hsp*::HLH-2::2xBFP] I; *nhr-67*(*syb509*[*nhr-67p*::NHR-67::GFP]) IV.
Strain, strain background (*C. elegans*)	DQM1135	This paper		*qyIs227*[*cdh-3p*::mCherry::moeABD] I; *lam-2*(*qy20*[*lam-2p*::LAM-2::mNeonGreen]) X; *lag-2*(*bmd202*[*lag-2p::*LAG-2::P2A::H2B::mTurquoise2^lox511^2xHA]) V; *lag-1*(*devKi208*[*lag-1*::mNeonGreen]) IV.
Strain, strain background (*C. elegans*)	JK3791	Phillips et al. (2007)		*qIs95[sys-1p::*Venus::SYS-1 + *pttx-3::DsRed]*
Strain, strain background (*C. elegans*)	NK1034	Matus et al. (2015)		*qyIs225*[*cdh-3p*::mCherry::moeABD] V; *qyIs7*[laminin::GFP] X.
Strain, strain background (*C. elegans*)	PHX509	Medwig-Kinney et al. (2020)		*nhr-67*(*syb509*[*nhr-67p*::NHR-67::GFP]) IV.
Strain, strain background (*C. elegans*)	PS5332	Green et al. (2008)		*syIs187*[*pes-10::7XTCF*-mCherry-*let-858(3'UTR)* + *unc-119(+)*]
Strain, strain background (*C. elegans*)	RW11476	Gerstein et al. (2010)		*unc-119*(*tm4063*) III; *stIs11476*[*nhr-67*::H1-wCherry + unc-119(+)].
Strain, strain background (*C. elegans*)	SV2114	van der Horst et al. (2019)		*pop-1*(*he335*[eGFP::loxP::*pop-1*]) I.
Strain, strain background (*C. elegans*)	TV27467	This paper		*nhr-67*(*wy1632*[*nhr-67p*::NHR-67::mNeonGreen::AID*::3xFLAG]) IV.
Strain, strain background (*C. elegans*)	TV27468	This paper		*nhr-67*(*wy1633*[*nhr-67p*::NHR-67::mScarlet-I::AID*::3xFLAG]) IV.
Recombinant DNA reagent	Plasmid: pTNM087	This paper		*lsy-22* sgRNA plasmid (AAACGAAGTGGATCAGCCAG)
Recombinant DNA reagent	Plasmid: pTNM088	This paper		*lsy-22*^SEC^TagRFP-T::AID repair plasmid
Recombinant DNA reagent	Plasmid: pTNM140	This paper		*lsy-22*^SEC^mNeonGreen::AID repair plasmid
Chemical compound, drug	1-Naphthaleneacetic acid, potassium salt (K-NAA)	PhytoTech Labs	N610	
Chemical compound, drug	Hygromycin B	Omega Scientific, Inc.	HG-80	
Chemical compound, drug	Levamisole hydrochloride	Sigma-Aldrich	31742	

Chemical compound, drug	Sodium azide	Sigma-Aldrich	S2002	
Software, algorithm	Adobe Illustrator	Adobe	Version 26.0.2	
Software, algorithm	Alpha Fold	Jumper et al. (2021); Varadi et al. (2021)	Version 2	
Software, algorithm	ApE – A Plasmid Editor	M. Wayne Davis	Version 2.0.61	
Software, algorithm	Fiji/ImageJ	Schindelin et al. (2012)	Version 2.0.0-rc-69/1.53e	
Software, algorithm	ggplot2	Tidyverse	Version 3.3.5	
Software, algorithm	Exon-Intron Graphic Maker	Nikhil Bhatla	Version 4	
Software, algorithm	JACoP (Just Another Colocalization Plugin)	Bolte and Cordelières (2006)	Version 2.1.1	
Software, algorithm	Metamorph	Molecular Devices	Version 7.10.3.279	
Software, algorithm	Rstudio	R	Version 1.4.1717	

513

514 **_C. elegans_ strains, culture, and nomenclature**

515 Methods for *C. elegans* culture and genetics were followed as previously
516 described (Brenner, 1974). Developmental synchronization for experiments was
517 achieved through alkaline hypochlorite treatment of gravid adults to isolate eggs (Porta-
518 de-la-Riva et al., 2012). L1 stage animals were plated on nematode growth media
519 plates and subsequently cultured at 20°C or 25°C. Heat shock-inducible transgenes
520 were activated by incubating animals on plates sealed with Parafilm in a 33°C water
521 bath for 2-3 hours. In the text and in figures, promoter sequences are designated with a
522 "*p*" following the gene name and gene fusions are represented by a double-colon (::)
523 symbol.

524

525 **CRISPR/Cas9 injections**

526 New alleles and single-copy transgenes were generated by homology directed
527 repair using CRISPR-based genome engineering. mScarlet::AID and mNeonGreen::AID
528 were inserted into the C-terminus of the *nhr-67* locus by injecting adult germlines with

529 Cas9 guide-RNA ribonucleoprotein complexes and short single-stranded
530 oligodeoxynucleotide donors, as previously described (Ghanta and Mello, 2020).
531 Successful integrants were identified through screening for fluorescence and by PCR.
532 The *lsy-22* locus was edited by injecting a Cas9 guide RNA plasmid and repair template
533 plasmid containing a self-excising cassette with selectable markers to facilitate
534 screening (Dickinson et al., 2015; Dickinson and Goldstein, 2016; Huang et al., 2021).
535 Repair templates used to tag *lsy-22* with TagRFP-T::AID and mNeonGreen::AID were
536 generated by cloning ~750-850 bp homology arms into pTNM063 and pDD312,
537 respectively (Ashley et al., 2021; Dickinson et al., 2015). All guide and repair sequences
538 used can be found in Supplemental Table 1.
539
540 **Existing alleles**
541 The GFP-tagged alleles of the pro-invasive transcription factors *(egl-43, fos-1,*
542 *hlh-2,* and *nhr-67)* and the TagRFP-T::AID-tagged *nhr-67* allele were generated in
543 preceding work (Medwig-Kinney et al., 2021, 2020). Recent micropublications describe
544 the P2A::H2B::mTurquoise2-tagged *lag-2* and mNeonGreen-tagged *lin-12* alleles used
545 in this study (Medwig-Kinney et al., 2022; Pani et al., 2022). The eGFP-tagged *pop-1*
546 allele and POPTOP reporter were previously published (Green et al., 2008; van der
547 Horst et al., 2019), as were the AID::BFP and mNeonGreen tagged alleles of *unc-37*
548 (Kurashina et al., 2021; Ma et al., 2021). GFP-tagged *ama-1* (Hills-Muckey et al., 2021)
549 as well as mKate2-tagged *hpl-1* and *hpl-2* (Patel and Hobert, 2017) were also
550 disseminated in prior publications. The single-copy transgenes expressing the CDK
551 sensor and TIR1 variants under ubiquitously expressed ribosomal promoters (*rps-27*
552 and *rpl-28*, respectively) as well as the tissue-specific GFP-targeting nanobody are
553 described in previous work (Adikes et al., 2020; Hills-Muckey et al., 2021; Smith et al.,
554 2022; Wang et al., 2017) and are located at neutral genomic sites, ttTi4348 or ttTi5605
555 (Frøkjær-Jensen et al., 2013). The same is true for the heat shock inducible constructs
556 for HLH-2 and NHR-67 (Medwig-Kinney et al., 2020). The cadherin *(cdh-3)* anchor cell
557 reporter and basement membrane (laminin) markers have already been characterized
558 (Keeley et al., 2020; Matus et al., 2010). The following mutant alleles were obtained
559 from the *Caenorhabditis* Genetics Center: *unc-37(e262wd26)* and *unc-37(wd17wd22)*

560 (Pflugrad et al., 1997), the latter of which was maintained using the chromosome I/III
561 balancer *hT2* (McKim et al., 1993). The genotypes of all strains used in this study can
562 be found within the Key Resources Table.
563
564 **Auxin inducible protein degradation**
565 The auxin inducible degron (AID) system was utilized to strongly deplete proteins
566 of interest (Zhang et al., 2015). AID-tagged alleles were paired with the *Arabidopsis*
567 *thaliana* F-box protein, transport inhibitor response 1 ($_{At}$TIR1), and treated with the
568 water-soluble auxin 1-Naphthaleneacetic acid (K-NAA) at 1 mM concentration (Martinez
569 et al., 2020). Auxin was added to nematode growth media plates according to
570 previously published protocols (Martinez and Matus, 2020), which were then seeded
571 with OP50 *E. coli*. To achieve robust depletion, synchronized L1 stage animals were
572 directly plated on auxin plates.
573
574 **RNA interference**
575 The RNAi clones targeting *pop-1* and *uba-1* as well as the corresponding empty
576 vector control (L4440) were obtained from the Vidal library (Rual et al., 2004). The RNAi
577 constructs targeting the pro-invasive transcription factors (*egl-43*, *fos-1*, *hlh-2*, and *nhr-*
578 *67*) and chromatin modifiers (*pbrm-1*, *swsn-4*, and *swsn-8*) are derived from the highly
579 efficient RNAi vector T444T (Sturm et al., 2018) and were generated in preceding work
580 (Medwig-Kinney et al., 2020; Smith et al., 2022). To avoid known AC/VU cell fate
581 specification defects caused by *hlh-2* perturbations, synchronized animals were grown
582 on OP50 until the L2 stage when they were shifted to *hlh-2* RNAi plates.
583
584 **Live cell imaging**
585 With the exception of the FRAP experiments shown in Figure 3, all micrographs
586 were collected on a Hamamatsu Orca EM-CCD camera mounted on an upright Zeiss
587 AxioImager A2 with a Borealis-modified CSU10 Yokagawa spinning disk scan head
588 (Nobska Imaging) using 405 nm, 440 nm, 488 nm, 514 nm, and 561 nm Vortran lasers
589 in a VersaLase merge and a Plan-Apochromat 100×/1.4 (NA) Oil DIC objective.
590 MetaMorph software (Molecular Devices) was used for microscopy automation. Several

591 experiments were scored using epifluorescence visualized on a Zeiss Axiocam MRM
592 camera, also mounted on an upright Zeiss AxioImager A2 and a Plan-Apochromat
593 100×/1.4 (NA) Oil DIC objective. For static imaging, animals were mounted into a drop
594 of M9 on a 5% Noble agar pad containing approximately 10 mM sodium azide
595 anesthetic and topped with a coverslip. For long-term time-lapse imaging, animals were
596 first anesthetized in 5 mM levamisole diluted in M9 for approximately 20 minutes, then
597 transferred to a 5% Noble agar pad and topped with a coverslip sealed with VALAP
598 (Kelley et al., 2017). For short-term time-lapse imaging, the pre-anesthetization step
599 was omitted, and animals were transferred directly into a drop of 5 mM levamisole
600 solution on the slide.
601
602 **Fluorescence recovery after photobleaching**
603 FRAP experiments were performed using an Acal BFi UV Optimicroscan
604 photostimulation device mounted on a spinning disk confocal system consisting of a
605 Nikon Ti2 inverted microscope with Yokogawa CSU-W1 SoRa spinning disk. Data were
606 acquired using a Hamamatsu ORCA Fusion camera, 60x 1.27 NA water immersion
607 objection, SoRa disk, and 2.8x SoRa magnifier. Single plane images were collected
608 every 1 second.
609
610 **Yeast one-hybrid**
611 The 276 bp fragment of the *nhr-67* promoter (Bodofsky et al., 2018) was cloned
612 into the pMW2 vector, linearized by BamHI digestion. Linearized plasmid was
613 transformed into the Y1H yeast strain (as described in Reece-Hoyes and Walhout,
614 2018). Transformed yeast was plated on SC-HIS plates for three days before being
615 transformed with the HLH-2 Gal4-AD plasmid. Three colonies from each transformation
616 plate were streaked onto SC-HIS-TRP +3-aminotriazole (3-AT) plates. Protein-DNA
617 interactions were determined by visible growth on 3-AT conditions with negative growth
618 in empty vector controls after three days. Plates were imaged on a Fotodyne
619 FOTO/Analyst Investigator/FX darkroom imaging station.
620
621 **Yeast two-hybrid**

622 Plasmids containing target proteins fused to GAL-4 DNA-binding-domain + LEU
623 and GAL-4 Activation Domain + TRP were co-transformed into the pJ69-4a Y2H yeast
624 strain as previously described (Reece-Hoyes and Walhout, 2018). Transformed yeast
625 was plated on SC-TRP-LEU plates for three days. Three colonies from each
626 transformation plate were streaked onto SC-HIS-TRP-LEU 3-AT plates. Protein
627 interactions were determined by visible growth on 3-AT conditions with negative growth
628 in empty vector controls after three days. Plates were imaged as described in the
629 previous section.
630
631 **Quantification of protein expression and cell cycle state**
632 Image quantification was performed in Fiji/ImageJ (Schindelin et al., 2012).
633 Protein expression was quantified by drawing a region of interest around the nucleus of
634 the cell of interest and measuring the mean gray value, then manually subtracting the
635 mean gray value of a background region of similar area to account for camera noise.
636 The CDK sensor was quantified as previously described (Adikes et al., 2020). Following
637 rolling ball subtraction (50 pixels), mean gray value is measured in a region of interest
638 drawn within the cytoplasm and one around the nucleus excluding the nucleolus. The
639 cytoplasmic-to-nuclear ratio correlates to CDK activity and is used to assess cell cycle
640 state (Adikes et al., 2020; Spencer et al., 2013). Movies were collected by acquiring z-
641 stacks at 5-minute intervals. Samples were time-aligned relative to anaphase. Cells that
642 did not undergo anaphase during the acquisition period were aligned based on their
643 DHB ratios. Animals that arrested in development (i.e., did not show evidence of
644 progressing through the cell cycle) were excluded from analysis.
645
646 **Colocalization analyses**
647 For colocalization analyses, single plane images were collected to avoid z drift
648 during acquisition and prevent photobleaching, which was often non-uniform between
649 red and green fluorophores. Micrographs were subject to background subtraction
650 (rolling ball radius = 50) followed by thresholding to segment punctae. Manders' overlap
651 coefficients (M) were calculated by measuring the extent that segmented punctae of
652 NHR-67 overlapped with that of other proteins using Just Another Colocalization Plugin

(JACoP) in Fiji/ImageJ (Bolte and Cordelières, 2006; Schindelin et al., 2012). Heterozygous animals for *nhr-67*::mScarlet and *nhr-67*::GFP were used as positive controls. These images were then re-analyzed following 90-degree rotation of one of the two channels being compared, resulting in random colocalization that served as a negative control.

Data visualization and statistical analyses

Representative images were processed using Fiji/ImageJ (Schindelin et al., 2012). Heat maps were generated using the Fire lookup table. Tests to determine statistical significance of data were conducted in RStudio and plots were generated using the R package ggplot2 (Wickham, 2016). Error bars represent the mean ± standard deviation. Schematics of gene loci were generated using sequences from WormBase (Harris et al., 2020) and the Exon-Intron Graphic Maker (http://wormweb.org/exonintron). Figures were assembled in Adobe Illustrator.

Acknowledgments

We are grateful to Dr. Derek Applewhite and Aidan Teran for advice on quantification of protein colocalization. Additionally, we thank Chris Zhao for constructive comments on the manuscript. Some strains were provided by the Caenorhabditis Genetics Center, which is funded by NIH Office of Research Infrastructure Programs (P40 OD010440).

Additional information

Funding

Funder	Grant reference number	Author
National Institutes of Health	R01GM121597	David Q. Matus
Damon Runyon Cancer Research Foundation	DRR-47-17	David Q. Matus

National Institutes of Health	F31HD100091	Taylor N. Medwig-Kinney
Stony Brook University	Presidential Critical Research Funds	Taylor N. Medwig-Kinney
National Institutes of Health	F30CA257383	Michael A. Q. Martinez
Human Frontier Science Program	LTF000127/2016-L	Callista Yee
Howard Hughes Medical Institute	Investigator	Kang Shen
National Institutes of Health	R01GM117406	Christopher M. Hammell
National Science Foundation	2217560	Christopher M. Hammell
National Institutes of Health	R35GM142880	Ariel M. Pani

Author contributions

Taylor N. Medwig-Kinney, Conceptualization, Formal Analysis, Investigation, Writing—original draft, Visualization, Supervision, Funding acquisition; Brian A. Kinney, Investigation, Writing—review and editing; Michael A. Q. Martinez, Investigation, Resources, Writing—review and editing; Callista Yee, Resources, Writing—review and editing; Sydney S. Sirota, Formal Analysis, Investigation, Resources; Angelina A. Mullarkey, Formal Analysis, Writing—review and editing; Neha Somineni, Formal Analysis, Resources; Justin Hippler, Formal Analysis, Resources; Wan Zhang, Resources; Kang Shen, Supervision; Christopher M. Hammell, Resources, Supervision, Writing—review and editing; Ariel M. Pani, Investigation, Writing—review and editing; David Q. Matus, Conceptualization, Supervision, Funding acquisition, Writing—review and editing

Author ORCIDs

693 Taylor N. Medwig-Kinney, https://orcid.org/0000-0001-7989-3291
694 Brian A. Kinney, https://orcid.org/0000-0001-5628-1436
695 Michael A. Q. Martinez, https://orcid.org/0000-0003-1178-7139
696 Callista Yee, https://orcid.org/0000-0002-2928-492X
697 Sydney S. Sirota, https://orcid.org/0000-0001-9990-3266
698 Angelina A. Mullarkey, https://orcid.org/0000-0002-5830-5347
699 Neha Somineni, https://orcid.org/0000-0001-5702-1695
700 Kang Shen, https://orcid.org/ 0000-0003-4059-8249
701 Christopher M. Hammell, https://orcid.org/0000-0002-5961-0976
702 Ariel M. Pani, https://orcid.org/0000-0002-9338-9750
703 David Q. Matus, https://orcid.org/0000-0002-1570-5025
704
705 **Figure legends** (supplementary figure legends are indented)
706
707 **Figure 1: Invasive AC fate correlates to high levels of NHR-67.** (A) Schematic of *C.*
708 *elegans* anchor cell (AC, magenta) and ventral uterine (VU, blue) cell fate specification
709 from the Z1 and Z4 somatic gonad precursor cell lineages (p, posterior daughter; a,
710 anterior daughter). (B) Micrographs depicting AC and VU cell differentiation over
711 developmental time. AC/VU precursors express LAG-2 (H2B::mTurquoise), which
712 eventually becomes restricted to the AC, whereas VU cells express LAG-1
713 (mNeonGreen) post-specification. The differentiated AC (*cdh-3p*::mCherry::moeABD)
714 then invades through the underlying basement membrane (LAM-2::mNeonGreen). (C-
715 D) Representative heat map micrographs (C) and quantification (D) of GFP-tagged
716 HLH-2 and NHR-67 expression in the AC and VU cells at the time of AC invasion. (E)
717 Expression of Notch (*lin-12*::mNeonGreen) and Delta (*lag-2*::P2A::H2B::mTurquoise2)
718 following RNAi-induced knockdown of *nhr-67* compared to empty vector control. (F)
719 Micrographs depicting the ectopic invasive ACs (*cdh-3p*::mCherry::moeABD,
720 arrowheads) and expanded basement membrane (*laminin*::GFP, arrows) gap observed
721 following heat shock induced expression of NHR-67 (*hsp*::NHR-67::2x-BFP) compared
722 to non-heat shocked controls. (G) Schematic summarizing AC and VU cell fates that
723 result from perturbations of NHR-67 levels. For all figures: asterisk (*), AC/VU

724 precursor; plus (+), VU precursor; solid arrowhead, AC; open arrowhead, VU cell;
725 arrows, basement membrane breach. Statistical significance determined by Student's t-
726 test (*$p > 0.05$, **$p > 0.01$, ***$p > 0.001$). Scale bars, 5 μm.
727
728 **Figure 1–figure supplement 1: Expression of pro-invasive transcription**
729 **factors EGL-43 and FOS-1 in the somatic gonad.** (A) Schematic of the AC
730 pro-invasive gene regulatory network comprised of four transcription factors:
731 EGL-43, FOS-1, HLH-2, and NHR-67. (B-C) Representative heat-map
732 micrographs (B) and quantification (C) of GFP-tagged EGL-43 and FOS-1
733 expression in the AC and VU cells.
734
735 **Figure 2: NHR-67 expression is downregulated in VU cells through direct**
736 **transcriptional regulation by HLH-2.** (A-B) Representative heat map micrographs (A)
737 and quantification (B) of NHR-67::GFP expression in VU cells following heat shock
738 induced expression of HLH-2 (2x-BFP) compared to non-heat shocked controls. (C)
739 Schematic of a 276 bp putative regulatory element within the promoter of *nhr-67*
740 (Bodofsky et al., 2018), annotated with the location of three hypomorphic mutations
741 (*pf2*, pf88, and *pf159*). (D) Yeast one-hybrid experiment pairing HLH-2 Gal4-AD prey
742 with the 276 bp fragment of the *nhr-67* promoter as bait on SC-HIS-TRP plates with and
743 without competitive inhibitor 3-AT (175 mM).
744
745 **Figure 2–figure supplement 1: Onset of expression and regulatory**
746 **interaction between NHR-67 and HLH-2 in the somatic gonad.** (A)
747 Micrographs depicting onset of GFP-tagged HLH-2 and a wCherry-labeled NHR-
748 67 transgene (inverted to aid visualization) in Z1.pp and Z4.aa cells at early (top)
749 and late (bottom) stages. (B-D) Representative micrographs (B) and
750 quantification (C-D) of GFP-tagged HLH-2 and TagRFP-T-tagged NHR-67 in AC
751 (C) and VU cells (D) following *uba-1(RNAi)* compared to control. Insets depict
752 different z planes of the same image.
753
754 **Figure 3: NHR-67 forms dynamic punctae in nuclei of VU cells.** (A) Heat-map

755 maximum intensity projection of NHR-67::GFP showing protein localization in the AC
756 and VU cells. (B) Spatial color coded projection of NHR-67::GFP punctae in VU, with
757 nuclear border indicated with a dotted line. (C) Schematic of DNA Helicase B (DHB)
758 based CDK sensor and its dynamic localization over the cell cycle. (D) Graphs depicting
759 CDK activity levels and corresponding cell cycle state (top), and percentage of cells
760 exhibiting NHR-67::GFP punctae (bottom) over time, aligned to anaphase. (E)
761 Representative time-lapse of NHR-67::GFP over the course of a cell cycle, with cell
762 membranes indicated with dotted lines. (F) Time-lapse depicting NHR-67::GFP punctae
763 fusion prior to cell division. Bottom panels are pseudo-colored. (G-H) Quantification (G)
764 and representative images (H) depicting fluorescence recovery of NHR-67::GFP
765 following photobleaching of individual punctae (arrow).
766
767 **Figure 3–figure supplement 1: Knock-in alleles of *nhr-67*.** (A) Representative
768 images of VU cells exhibiting punctae formed by NHR-67 tagged with GFP,
769 mNeonGreen, mScarlet-I, and TagRFP-T. (B) Schematics of the new
770 endogenously tagged loci generated in this paper for *nhr-67*. Scale bar, 100 base
771 pairs (bp).
772
773 **Figure 4: Groucho homologs LSY-22 an UNC-37 colocalize with NHR-67 punctae**
774 **and repress invasive differentiation in VU cells.** (A) Co-visualization of NHR-67 with
775 RNA Polymerase II (GFP::AMA-1), HP1 heterochromatin proteins (HPL-1::mKate2 and
776 HPL-2::mKate2), and Groucho homologs (TagRFP-T::LSY-22 and mNeonGreen::UNC-
777 37) in VU cells using endogenously tagged alleles. (B) Quantification of colocalization,
778 with plot reporting Manders' overlap coefficients compared to negative controls (90
779 degree rotation of one channel) and positive controls. (C) Schematic of the auxin
780 inducible degron (AID) system, where *At*TIR1 mediates proteasomal degradation of AID-
781 tagged proteins in the presence of auxin. (D) Representative images of phenotypes
782 observed following individual AID-depletion of UNC-37 and LSY-22 compared to control
783 animals without AID-tagged alleles. Insets depict different z planes of the same image.
784
785 **Figure 4–figure supplement 1: Knock-in alleles of *lsy-22*.** Schematics of the

786 new endogenously tagged loci generated in this paper for *lsy-22*. Scale bar, 100
787 base pairs (bp).
788
789 **Figure 4–figure supplement 2: UNC-37 mutants show ectopic expression of**
790 **AC markers.** Ectopic expression of AC marker (*cdh-3p*::mCherry::moeABD) in
791 hypomorphic (*unc-37(e262wd26)*) and null (*unc-37(wd17wd22)*) alleles of *unc-37*
792 compared to wild-type *unc-37*. Insets depict different z planes of the same image.
793
794 **Figure 5: POP-1 associates with repressive condensates in the absence of Wnt**
795 **signaling.** (A-B) Expression of mNeonGreen::UNC-37 and mNeonGreen::LSY-22 (A)
796 and eGFP::POP-1 (B) in the AC/VU precursors pre-specification (left), as well as the AC
797 and VU cells post-specification (right). (C) Quantification of UNC-37, LSY-22, and POP-
798 1 expression at the time of AC invasion. (D) Co-visualization of NHR-67::mScarlet-I and
799 EGFP::POP-1 in the VU. (E) Quantification of POP-1 and NHR-67 colocalization, with
800 plot reporting Manders' overlap coefficient compared to negative and positive controls.
801 (F) Representative micrographs showing expression of POPTOP, a synthetic *pop-1*-
802 activated reporter construct, in wild-type ACs, VU cells, and their precursors. Insets
803 depict different z planes of the same image. (G-H) Micrographs (G) and quantification
804 (H) of eGFP-tagged POP-1 expression in proliferative ACs following RNAi depletion of
805 *nhr-67* compared to empty vector control.
806
807 **Figure 5–figure supplement 1: Expression of LSY-22, UNC-37, and POP-1**
808 **over developmental time.** (A-B) Developmental series (A) and quantified
809 expression (B) of mNeonGreen::UNC-37, mNeonGreen::LSY-22, and
810 eGFP::POP-1 expression in the AC/VU precursors, AC, and VU cells over time.
811 Following AC/VU cell specification, animals are staged by the division of the
812 underlying primary vulval precursor cells (1° VPCs).
813
814 **Figure 5–figure supplement 2: POP-1 repressive function in VU cells is**
815 **distinct from activator function in distal somatic gonad.** (A) Schematics
816 representing the dual functions of POP-1. In the presence of Wnt signaling, POP-

817 1 binds to its co-activator β-catenin (e.g., SYS-1) and activates transcription of its
818 target genes. In the absence of Wnt signaling, POP-1 binds to its co-repressor
819 Groucho (UNC-37) and represses transcription of its target genes. (B)
820 Representative micrographs of eGFP::POP-1 and POPTOP (*pes-10*::7x-
821 TCF::mCherry) expression in the AC, dorsal uterine cells (DU),
822 spermatheca/sheath cells (SS), and VU cells. (C) Schematic of SYS-1 (β-
823 catenin) expression in the Z1/Z4 lineage (based on Philips et al., 2007).
824
825 **Figure 5–figure supplement 3: POP-1 expression is regulated by the cell**
826 **cycle-dependent pro-invasion pathway.** (A-B) Representative micrographs of
827 eGFP::POP-1 and POPTOP (*pes-10*::7x-TCF::mCherry) following RNAi-induced
828 knockdown of pro-invasive transcription factors and chromatin modifiers
829 compared to control AC and VU cells. (B) Quantification of eGFP::POP-1
830 expression in ACs following RNAi treatments. Here, the presence of multiple ACs
831 are the result of failure of the AC to exit the cell cycle.
832
833 **Figure 6: Ectopic ACs arise through VU-to-AC cell fate transformation.** (A)
834 Representative images of ectopic AC (*cdh-3p*::mCherry::moeABD; LAG-
835 2::P2A::H2B::mTurquoise2) phenotypes observed following RNAi depletion of POP-1.
836 Schematics (right) depict potential explanations for observed phenotypes. (B)
837 Expression of AC markers and a VU cell marker (LAG-1::mNeonGreen, inverted to aid
838 visualization) in *pop-1(RNAi)* treated animals over time. (C) Quantification of LAG-2
839 (magenta) and LAG-1 (blue) expression in transdifferentiating cells produced by *pop-*
840 *1(RNAi)* over time.
841
842 **Figure 6–figure supplement 1: POP-1 functions to regulate AC/VU cell fates**
843 **post-specification.** (A) Schematic of the anti-GFP nanobody protein
844 degradation system (based on Wang et al., 2017). (B) Micrographs
845 demonstrating that the anti-GFP nanobody (driven under the *egl-43L* promoter) is
846 not expressed pre-specification or even shortly after when the presumptive AC
847 begins to express its differentiated cell reporter (*cdh-3*). (C) With decreased

848 levels of *pop-1*, a low penetrance (~7%) of multi-AC phenotypes were observed.

849

850 **Figure 6–figure supplement 2: Ectopic ACs resulting from *pop-1***
851 **perturbation express VU cell markers.** Expression of AC markers (*cdh-*
852 *3p*::mCherry::moeABD; LAG-2::P2A::H2B::mTurquoise2) and VU marker (LAG-
853 1::mNeonGreen) in *pop-1(RNAi)* treated animals compared to empty vector
854 control.

855

856 **Figure 7: NHR-67 binds to UNC-37 through IDR-mediated protein-protein**
857 **interaction.** (A) Predicted structure of NHR-67 generated by AlphaFold. (B) Measure of
858 intrinsic disorder of NHR-67 using the PONDR VSL2 prediction algorithm. (C)
859 Schematic of NHR-67 protein coding sequences used for Yeast two-hybrid experiments
860 with reference to its intrinsically disordered region (IDR, magenta), DNA binding domain
861 (DBD, green), and ligand binding domain (LBD, cyan). Scale bar, 10 amino acids. (D)
862 Yeast two-hybrid experiment shows pairing of UNC-37 with either full-length NHR-67 or
863 the IDR alone allows for yeast growth in the presence of competitive inhibitor 3-AT (20
864 mM). (E) Summary model of the roles of NHR-67, UNC-37, LSY-22, and POP-1 in
865 maintenance of AC and VU cell fate.

866

867 **Figure 7–figure supplement 1. NHR-67 exhibits protein-protein interaction**
868 **with UNC-37.** Yeast two-hybrid experiment pairing UNC-37 and NHR-67 Gal4-
869 AD prey with LSY-22, NHR-67, and POP-1 Gal4-DBD bait on SC-HIS-TRP-LEU
870 plates with and without competitive inhibitor 3-AT (20 mM).

871

872 **Supplemental Table 1: Sequences**

Method	Reagent	Sequence
CRISPR	*lsy-22* sgRNA	AAACGAAGTGGATCAGCCAG
CRISPR	*lsy-22* left homology arm	GAGACCAGGCAGCATATTTTTGTGCAAACTCCTTTGAAATTATTGTTATT ACAGATTTTTTGAAATTAGTAATTTCGGAAGTCTCCAAATTCTTAAAATGT CCTTTCCTTCCTTCGTCTCCTTCTCACTTTCCCGGCGGTAATTGGTTTTG GCGTAGAACATGGCGCCGGCGCAAACACATTGACGCAAAAGTTCACAA TTTAAAAGACCGTGTAAACAAGACCTCCTCCCCCTGTCCGCTCGTCTTC

		TCAAAGAACTTTTTTATCTTTTCCGTTGTTTTATCGCTTTTCTCATAATAA AAATAAAAATCGTCGTTGAAGAAATAAAATGGGCCCCGCCGTTGGTGTG TGTGTGCCATCACAACCATCAATTCAAACTTTGTTTTATTTCTACTTTTTT GCAGCTCATTGCTCCGTGACGGATTCAAATTGTTGTTTTTCTTCGCGAC AAACAAGAAAGACTCTGGAATTGTATCGTTTTCGAATTTTTAAAATTTGG AATTTTTGATCGCCTGTCGATCAACCCCCGTCTACAATCACGTCGGACC AACGAAGATTCGCGAATCCGAACTTCTCGCATCCTAGCTCGAGTAGTTC AAGGGAAAAGTAGGTTTTTATTATATTTTAAAAGTAAAAGATTTGTTGAC AAATAGTTGAAAATGGTATTCTAAAAGTTGAGAAAATTAAAAATATGAAA GGTTCACTAGAGGCATATTTTTCATTTTGAAAGTATCAAAATAAATTCAA AAACAGCGTTTAATTTCTTTTAGAAAACTAGAAATTCGAAAACTAGAAAT TGGTGAATATGAACAGTATTTAATTTATATTTTAGTAGGAAACGAAGTGG ATCAGCCAGCGCA
CRISPR	*lsy-22* right homology arm	ATGTCACTAGCAGATCATATTGATGCAATCAAAAAAGAAATGACAAGTCT ATCGAGCCAATTCAACTCGAATAAATCAGAACTTGAACGATCAAAACAG GATTTATCATCAATGCAACTACAAATGCAACAACAAATGAACGATTCAGT ACAGCAGGACCTCCAGAAAGCTCATGATACATCGAAGAAATTAGATAAT CTTGCAAGGACGTTTCTTGCATTAATTACTGATCCATCGCAACAATCACA ATTATTAGCGGAATTTGAATCAATTTCCAAGAACGGAACACCTCAAATG CCAGTGATGACACCTCCAATGATGAATGCAGTTGCTGCAATGCAACCAC ATATGATGATGAGGAATCCAATGCTGAATGCAATGGGTGGAGCATCAC CACGTGTTTCTGGAAAAGGTGGAGCTCCACAAAACGGTGGAATGAATG GGATGTCGATGATGCAGCACATGCAAATGCAAGCATTCCAGGCACAAA TGATGCAAGCTCAAATGTTTCAGCAGATGCCGATGATGATGCCAGGGA TGGTTCCTGGAATGCCACCGGGAATGGCTGGATTGCCTGGAATGATGC CACCGAATAATATGGCAGCTGCAATGCAACATTTTAATGCGGTAAGTGT TAACTATTATTCAAAATGTTGAGATTAAATTATGTTTATCGTAATTTTCTC TTAGGGGCACGGATTTATCCAGATGGGGTCGGCGGGGAAAAATCTATG ATAGT
CRISPR	*nhr-67* sgRNA	AGAGAGTGTTAATGTTGAAG
CRISPR	*nhr-67* left homology arm	TTCCTCAACTCAGCCTTCATCGGCATCATCCCCTTCCTCTTCAAGACCA CGTCATTCGATTCGATCAATAACTGAATTATTATCAATTCAAGAAGAGGA AAGCGTGAACGTGGAGGAAGTG
CRISPR	*nhr-67* right homology arm	TAAATAGTAAATTCATGTTTCATATACAGTAACTCAATTATTCTAAGTATC TCTTTTCATTGTCTTTTTCACTCCGTTTCTTGCCTCGCCCGGATTTTCATT GGATTTTGATTTATACTT
Y1H	276 bp *nhr-67* promoter element	ACCATTTCGCTAAGTTTTCCAAAAGTTCACACCTGTATGACCCTCGTCTG TCTATCTCTCTTCAACGACCTTTTCCTGCATCGTTCTCGATATTGCGTAA AATCCCAACACATTGTCTTACTCTTGGGTAAAATCGAGAAAAAAAAGTAT TTTTGATTGCGTAAGCATCAAAATGAAATGCAGGTGTTCACCACTAAAAT GAAATGGAGGTCATGTTCGTACCCTGTGGTACAAGCCACAGAGAGTTC AATTTATATGATGAGCATTTGAAGAATT
Y2H	LSY-22 cDNA	ATGTCACTAGCAGATCATATTGATGCAATCAAAAAAGAAATGACAAGTCT ATCGAGCCAATTCAACTCGAATAAATCAGAACTTGAACGATCAAAACAG GATTTATCATCAATGCAACTACAAATGCAACAACAAATGAACGATTCAGT ACAGCAGGACCTCCAGAAAGCTCATGATACATCGAAGAAATTAGATAAT CTTGCAAGGACGTTTCTTGCATTAATTACTGATCCATCGCAACAATCACA ATTATTAGCGGAATTTGAATCAATTTCCAAGAACGGAACACCTCAAATG

		CCAGTGATGACACCTCCAATGATGAATGCAGTTGCTGCAATGCAACCAC ATATGATGATGAGGAATCCAATGCTGAATGCAATGGGTGGAGCATCAC CACGTGTTTCTGGAAAAGGTGGAGCTCCACAAAACGGTGGAATGAATG GGATGTCGATGATGCAGCACATGCAAATGCAAGCATTCCAGGCACAAA TGATGCAAGCTCAAATGTTTCAGCAGATGCCGATGATGATGCCAGGGA TGGTTCCTGGAATGCCACCGGGAATGGCTGGATTGCCTGGAATGATGC CACCGAATAATATGGCAGCTGCAATGCAACATTTTAATGCGTTTCAGCA AATGGCCGCCGCTGCATCGGTAGCAGTTTCTACACCATCAAGGAATCC ATCAACATCTGGAGCCGCTTCTCGAACACGAACTCCATTAACCACATCA GCCACGAATTCACCTCGACCCACCACAGAACCAACGATTAAAGAAGAA GAACCACAGACAATGGAACATGATGTAGCTGCTGCTGTGGCCGCAACT ACTGCTACTGCAACAATCAAACAAGAAGAAAATTCGACAGTGGCGGTTG CTTGA
Y2H	NHR-67 cDNA	ATGATGACCGCTGTCTCTCAAATGTCTGTCCCATCCTCCCGTATCCTTC TTGACGTCGACTGCCGTGTTTGCGAGGACCACTCTTCTGGAAAGCACT ACTCTATCTTCTCTTGCGATGGATGCGCCGGATTCTTCAAGCGCTCTAT CCGCCGCCACCGCCAGTACGTTTGTAAGAACAAGGGATCTCCATCTGA GGGACAATGCAAGGTTGATAAGACTCACCGTAACCAATGCCGCGCCTG CCGTCTTCGCAAGTGCCTTGAGATCGGAATGAACAAGGACGCCGTTCA ACACGAGCGCGGACCACGCAACTCTTCTCTTCGCCGCCAACAAATGAT GTTCGACCACGGATCTTCCCCAAACTCTCCAGAGATGGGATCTGAGTC CGACGCTATCATCCTCCCAACCTCTTCTATGAACCGTGATACCGTCGCT GGAACCGCCGCCCGTATCTTCTTCGCTCTCGTCGGATTCTGCCAAAAC CCACTTAACGGAGTTCCAAAGGAGCGCCAGATGACTATGTTCCAGCAA AACTGGGCTGCCCTCCTCGTCCTTCACGCTACCGAGACCCGCGCTATC ACCTCCAAGCAAATCCGCACCGAGACCATCTCTGGATCTTCTGAGCAA CGTAACGCTGTCGCCAACGCTTTCGAGATCATCGAGCGTCTTCAACTTG ACAACCGCGAGTACATGATGCTTAAGCACTTCACCATGTGGCGCGACA CCCCATCTGCTATCCAAATCGTTTTCCAACTTGCTTCCATCCAAAACTTC ACTCACCGCACTGAGCCAACTCGCTACATCCAGTGCATCAACGCTATC GCTGCCATCCCAACTACCTCTATCATCGACGTCCTTTTCCGTCCATCTA TCGGATCTGCCTCTATGCCACGTCTCATCCAGGATATGTTCAAGCCACC ACAGCAGCCAACCCCAACCTCTCTTTTCCCAATGGCTAATTTCAACCTT AACTTCCTTCTTAAGCAAGAGAAGACTGAGACCGAGGAAGGAGAGGAC ATCGAGGAGGAGGACGACGCTACCTCTTCTAACCAATTCGACGAGAAC TCCTCCACCGACGACCGTTCCGTCGGAGAGCTTGACCCAGTCCAACTC TTCCTTGCCCTCAACTCTTCTACCCAACCATCTTCTGCTTCTTCTCCATC TTCCTCTCGCCCACGTCACTCTATCCGTTCTATCACCGAGCTTCTTTCTA TCCAAGAGGAGGAGTCTGTCAACGTCGAGGAGGTCTAG
Y2H	NHR-67 (ΔIDR) cDNA	ATGATGACCGCTGTCTCTCAAATGTCTGTCCCATCCTCCCGTATCCTTC TTGACGTCGACTGCCGTGTTTGCGAGGACCACTCTTCTGGAAAGCACT ACTCTATCTTCTCTTGCGATGGATGCGCCGGATTCTTCAAGCGCTCTAT CCGCCGCCACCGCCAGTACGTTTGTAAGAACAAGGGATCTCCATCTGA GGGACAATGCAAGGTTGATAAGACTCACCGTAACCAATGCCGCGCCTG CCGTCTTCGCAAGTGCCTTGAGATCGGAATGAACAAGGACGCCGTTCA ACACGAGCGCGGACCACGCAACTCTTCTCTTCGCCGCCAACAAATGAT GTTCGACCACGGATCTTCCCCAAACTCTCCAGAGATGGGATCTGAGTC CGACGCTATCATCCTCCCAACCTCTTCTATGAACCGTGATACCGTCGCT GGAACCGCCGCCCGTATCTTCTTCGCTCTCGTCGGATTCTGCCAAAAC CCACTTAACGGAGTTCCAAAGGAGCGCCAGATGACTATGTTCCAGCAA AACTGGGCTGCCCTCCTCGTCCTTCACGCTACCGAGACCCGCGCTATC ACCTCCAAGCAAATCCGCACCGAGACCATCTCTGGATCTTCTGAGCAA CGTAACGCTGTCGCCAACGCTTTCGAGATCATCGAGCGTCTTCAACTTG

		ACAACCGCGAGTACATGATGCTTAAGCACTTCACCATGTGGCGCGACA CCCCATCTGCTATCCAAATCGTTTTCCAACTTGCTTCCATCCAAAACTTC ACTCACCGCACTGAGCCAACTCGCTACATCCAGTGCATCAACGCTATC GCTGCCATCCCAACTACCTCTATCATCGACGTCCTTTTCCGTCCATCTA TCGGATCTGCCTCTATGCCACGTCTCATCCAGGATATGTTCAAGCCACC ACAGCAGTAG
Y2H	NHR-67 IDR cDNA	ATGCCAACCCCAACCTCTCTTTTCCCAATGGCTAATTTCAACCTTAACTT CCTTCTTAAGCAAGAGAAGACTGAGACCGAGGAAGGAGAGGACATCGA GGAGGAGGACGACGCTACCTCTTCTAACCAATTCGACGAGAACTCCTC CACCGACGACCGTTCCGTCGGAGAGCTTGACCCAGTCCAACTCTTCCT TGCCCTCAACTCTTCTACCCAACCATCTTCTGCTTCTTCTCCATCTTCCT CTCGCCCACGTCACTCTATCCGTTCTATCACCGAGCTTCTTTCTATCCA AGAGGAGGAGTCTGTCAACGTCGAGGAGGTCTAG
Y2H	POP-1 cDNA	ATGATGGCCGACGAAGAGCTCGGCGATGAGGTGAAGGTGTTCCGTCG GGATGAGGATGCTGACGATGATCCAATGATTAGTGGTGAAACGTCAGA ACAACAGTTAGCCGATGATAAAAAAGAAGCTGTAATGGAAGCAGAATTA GACGGTGCCGGTCGAAATCCATCGATTGATGTGTTAAAAAGTGCATTTC CAAAAGTCGAACCAATGTCACCATCGTTTCCCGGTTTAATGTCACACTT CAGTCCTGGATACTCGGCAGCTGCTTTACCCATGTTTATGCCTCTATTT ATGAATCCATACGCAGCAGCACTACGATCACCAAGCCTGATGTTTCCAA TGGGAGCAATGAGCCCCACATTTCCAATGTTCCCGCCAAGTCCTGTCTA TGGAGCAGCAATCGCTGCGGCAGCCGCCAAACAACACTTTGAGAATAT GGCTCCACTGAACATGCGAGCCGGTCATCCAATGAATCAGATGGGAAT GCCACCATACATGCATCCATCATCAATGGCTCCACAGAATGTCGATCGA AGGGCTCAAGGAGGTGGAAAAGCGAAGAAGGATGATCATGTGAAGAAG CCATTAAACGCGTTCATGTGGTTTATGAAGGAAAATCGAAAAGCACTGC TGGAAGAGATTGGAAATAATGAGAAACAGAGTGCAGAGTTGAATAAAGA GCTTGGAAAGAGGTGGCATGATTTGTCGAAGGAAGAACAGGCGAAATA TTTTGAAATGGCAAAGAAGGATAAGGAAACACACAAGGAACGGTATCC GGAGTGGTCGGCGCGGGAAAATTATGCGGTTAATAAGAAAAAGACGAA GAAACGAAGGGATAAGAGTATTCCATCGGAGAACAACGATCAGAAGAA GTGCCGAGCCAGATTCGGAGTTAACAACACAGAAATGTGGTGTAAATTC TGCAAGCGGAAGAAGAAGTGCGAGTACGCAACTGATCGTTCGGGCGG TTCCGATATAACTGACAGTCAGGATGGACGAGGTACAAGTGGTGCGTA TAGCAGTAGCTCGGAGAGCCCATCACCAAAGGCAAACGCTGGAATTGC ACTGACCACACAGCAGCAGCAAGCAGCAATGATGCATACGATGTTGAT GCAAATGCGTCTAGGATCGACGACGGGAGCATCGACGCACGTTCCATC ACCACTGGCGTCCTCGTCGGCAGGCAGGAGTCCGCTGGATGCGAACG CGTCGGATTCGGAATCTGATGTTGAGGAGGAGGAAGACGAGCAGATTG ATCCGACGGTTATGCAGCAGACACATGATATGCTTATGCAGGAATCGAT GTGTACTATTTAA
Y2H	UNC-37 cDNA	ATGAAGGCATCGTATCTGGAAACCCTCGATCGAATCAAAGACGAGCAT GCGGAAATGTCGAAGCATGTCAACCAGCAACGATCGGATATCGAAAAG GTTGCGTTAGAGAAAGAAAATATGAATAGATCGTATATGACGTACGCTG AAGTATCAAATACTCTTCGTAGCGATCTTCGAAAAGCAGAAGAAATCAA CAAACGCCTTCAGGAATTCATCATGCAATCGTTGGCTCCTCAACTATCT CAAGATAATCAAGCAAACTGCCTCGCCGCACTGGAAGCTTTCAAAACC GCATCACCACGTGAAAATGGAAATGGAGCACCAGCACTTCCACCAGGT TTTCCTCCCGGTGCAGCTGGAATGCTTGGAATGATGCCAAATATGCCAT TCGGAATGAGCCCTGCAATGAGTCAACTATTCAATCAATTCGCATCACC ACATGTCAACGGTGGAGATGGAGCCGGTGGAAGTTCTGGAGGTGCAA GTGAAGCGAAAAAGGCCAAGCTGGAAGATCCAGATGATGGAGAACTTG

		AGATTGATGTCACAAATGATGATCATCCAAGTACTGCATCAAATGGAGG CGCAGCTAATAAAAATGGAAGAGATAGCACAAATAGTGTTGCCTCATCG GGAGCATCTACACCGAGCATCGCATCAAATTCTAGAGCAAGACAACAA CAGCAGCCACTCGCTGGGCTTCAAGGATTGGAGCAAATGAACTTTTTA GCTGGATTCAATCCAAATCTTCTCCGACAAGCTAGTGCTGCTGGAGGAT TCAACTTTTTGAATGATCCCCATGCACAGGCCCGTCTTGCAGCTGCCAT CGGGCAAATCGGTAGCAGACCGGCCTATTCATTCAAAATTGTGGACGG TGGAGTTCCAACACCTACATCCTTCCCTCCAGATGCACAGAAAGGTCCC GGAATTCCGACAGGTCTCAAGAAGAAAATGGAATTAAATCACGGAGAA GTAGTTTGTGCGGCCACAATTTCCCGTGATAACAGTCGTGTTTATACTG GTGGAAAAGGATGTGTTAAGATCTGGGATGTCAAAGAATCAGATATTTC TGGCGCAACGGTTGTGAATCGGCCTCCAATTGCATCCTTGGATTGTCTC AAAGAGAACTATATTAGATCTTGTAAACTCTTTGAAGATGGAAATACACT TCTGATTGGAGGAGAAGCCAGTACTGTTGCTCTTTGGGATCTTACAACT GAAACAAAAACTTTGGACTTGGAAACTGATTCACAAGCATGCTACGCGT TGGCGATGTCACCAGATGAGAAATTATTGTTCGCATGTCTTGCTGATGG AAATATCCTCATTTATGATATCCATAATAAGGTGAAAGTTGGAACCCTAC CTGGACATCAAGATGGAGCATCATGTCTCGATCTCTCAAAAGATGGTAC AAAGCTCTGGTCAGGTGGTCTTGACAATTCTGTTAGATGCTGGGATCTT GCACAACGAAAGGAAGTTGCGAAGCATGATTTTGCGAGCCAAGTTTTCT CTCTTGGATGTTGTCCAAATGATGAATGGGTGGCTGTTGGTATGGAGAA TAATTATGTCGAGGTTCTGTCAACAACTGGAAAAGAAAAGTATCAATTGA CACAACACGAATCATGCGTCCTTTCGCTCAAATTTGCGCATTCCGGAAA GTTCTTCATTTCAACTGGAAAGGACAATGCTCTCAACGCCTGGCGTACT CCATACGGAGCATCACTCTTTCAACTAAAAGAGAACAGCTCCGTTCTCT CATGTGACATCTCATTCGACGACTCACTCATTGTCACTGGATCAGGGGA GAAGAAGGCAACTCTCTATGCAGTTGAATATTAA

References

Adikes RC, Kohrman AQ, Martinez MAQ, Palmisano NJ, Smith JJ, Medwig-Kinney TN, Min M, Sallee MD, Ahmed OB, Kim N, Liu S, Morabito RD, Weeks N, Zhao Q, Zhang W, Feldman JL, Barkoulas M, Pani AM, Spencer SL, Martin BL, Matus DQ. 2020. Visualizing the metazoan proliferation-quiescence decision in vivo. *Elife* **9**:1–74. doi:10.7554/eLife.63265

Ashley G, Duong T, Levenson MT, Martinez MAQ, Johnsen LC, Hibshman JD, Saeger HN, Palmisano NJ, Doonan R, Martinez-Mendez R, Davidson B, Zhang W, Ragle JM, Medwig-Kinney TN, Sirota SS, Goldstein B, Matus DQ, Dickinson DJ, Reiner DJ, Ward JD. 2021. An expanded auxin-inducible degron toolkit for Caenorhabditis elegans . *Genetics*. doi:10.1093/genetics/iyab006

Attner MA, Keil W, Benavidez JM, Greenwald I. 2019. HLH-2/E2A Expression Links Stochastic and Deterministic Elements of a Cell Fate Decision during C. elegans Gonadogenesis. *Curr Biol* **29**:1–7. doi:10.1016/j.cub.2019.07.062

Bekas KN, Phillips BT. 2022. unc-37/Groucho and lsy-22/AES repress Wnt target genes in C. elegans asymmetric cell divisions. *bioRxiv*.

Benavidez JM, Kim JH, Greenwald I. 2022. Influences of HLH-2 stability on anchor cell fate specification during Caenorhabditis elegans gonadogenesis. *G3: Genes|Genomes|Genetics*.

Bodofsky S, Liberatore K, Pioppo L, Lapadula D, Thompson L, Birnbaum S, McClung G, Kartik A, Clever S, Wightman B. 2018. A tissue-specific enhancer of the C. elegans

895 nhr-67/tailless gene drives coordinated expression in uterine stem cells and the
896 differentiated anchor cell. *Gene Expr Patterns* **30**:71–81.
897 doi:10.1016/j.gep.2018.10.003
898 Boija A, Klein IA, Sabari BR, Dall'Agnese A, Coffey EL, Zamudio A V., Li CH, Shrinivas
899 K, Manteiga JC, Hannett NM, Abraham BJ, Afeyan LK, Guo YE, Rimel JK, Fant
900 CB, Schuijers J, Lee TI, Taatjes DJ, Young RA. 2018. Transcription Factors
901 Activate Genes through the Phase-Separation Capacity of Their Activation
902 Domains. *Cell* **175**:1842-1855.e16. doi:10.1016/j.cell.2018.10.042
903 Bolte S, Cordelières FP. 2006. A guided tour into subcellular colocalization analysis in
904 light microscopy. *J Microsc* **224**:213–232. doi:10.1111/j.1365-2818.2006.01706.x
905 Boxem M, Maliga Z, Klitgord N, Li N, Lemmens I, Mana M, de Lichtervelde L, Mul JD,
906 van de Peut D, Devos M, Simonis N, Yildirim MA, Cokol M, Kao HL, de Smet AS,
907 Wang H, Schlaitz AL, Hao T, Milstein S, Fan C, Tipsword M, Drew K, Galli M,
908 Rhrissorrakrai K, Drechsel D, Koller D, Roth FP, Iakoucheva LM, Dunker AK,
909 Bonneau R, Gunsalus KC, Hill DE, Piano F, Tavernier J, van den Heuvel S, Hyman
910 AA, Vidal M. 2008. A Protein Domain-Based Interactome Network for C. elegans
911 Early Embryogenesis. *Cell* **134**:534–545. doi:10.1016/j.cell.2008.07.009
912 Brangwynne CP, Eckmann CR, Courson DS, Rybarska A, Hoege C, Gharakhani J,
913 Jülicher F, Hyman AA. 2009. Germline P Granules Are Liquid Droplets That
914 Localize by Controlled Dissolution/Condensation. *Science (80-)* **324**:1729–1732.
915 Brenner S. 1974. The genetics of *Caenorabditis elegans*. *Genetics* **77**:71–94.
916 doi:10.1016/S0047-2484(78)80101-8
917 Brumbaugh J, Stefano B Di, Hochedlinger K. 2019. Reprogramming : identifying the
918 mechanisms that safeguard cell identity. *Development* **146**:1–17.
919 doi:10.1242/dev.182170
920 Calvo D, Victor M, Gay F, Sui G, Po-Shan Luke M, Dufourcq P, Wen G, Maduro M,
921 Rothman J, Shi Y. 2001. A POP-1 repressor complex restricts inappropriate cell
922 type-specific gene transcription during Caenorhabditis elegans embryogenesis.
923 *EMBO J* **20**:7197–7208. doi:10.1093/emboj/20.24.7197
924 Cho WK, Spille JH, Hecht M, Lee C, Li C, Grube V, Cisse II. 2018. Mediator and RNA
925 polymerase II clusters associate in transcription-dependent condensates. *Science*
926 *(80-)* **361**:412–415. doi:10.1126/science.aar4199
927 Chong S, Dugast-Darzacq C, Liu Z, Dong P, Dailey GM, Cattoglio C, Heckert A, Banala
928 S, Lavis L, Darzacq X, Tjian R. 2018. Imaging dynamic and selective low-
929 complexity domain interactions that control gene transcription. *Science (80-)* **361**.
930 doi:10.1126/science.aar2555
931 Davis RL, Weintraub H, Lassar AB. 1987. Expression of a single transfected cDNA
932 converts fibroblasts to myoblasts. *Cell* **51**:987–1000. doi:10.1016/0092-
933 8674(87)90585-X
934 Dickinson DJ, Goldstein B. 2016. CRISPR-based methods for caenorhabditis elegans
935 genome engineering. *Genetics* **202**:885–901. doi:10.1534/genetics.115.182162
936 Dickinson DJ, Pani AM, Heppert JK, Higgins CD, Goldstein B. 2015. Streamlined
937 genome engineering with a self-excising drug selection cassette. *Genetics*
938 **200**:1035–1049. doi:10.1534/genetics.115.178335
939 Flowers EB, Poole RJ, Tursun B, Bashllari E, Pe'er I, Hobert O. 2010. The Groucho
940 ortholog UNC-37 interacts with the short Groucho-like protein LSY-22 to control

941 developmental decisions in C. elegans. *Development* **137**:1799–1805.
942 doi:10.1242/dev.046219
943 Frøkjær-Jensen C, Davis MW, Ailion M, Jorgensen EM. 2013. Improved Mos1-mediated
944 transgenesis in C. elegans. *Nat Meth* **9**:117–118. doi:10.1038/mp.2011.182.doi
945 Fukushige T, Krause M. 2005. The myogenic potency of HLH-1 reveals wide-spread
946 developmental plasticity in early C. elegans embryos. *Development* **132**:1795–
947 1805. doi:10.1242/dev.01774
948 Ghanta KS, Mello CC. 2020. Melting dsDNA donor molecules greatly improves
949 precision genome editing in caenorhabditis elegans. *Genetics* **216**:643–650.
950 doi:10.1534/genetics.120.303564
951 Gilleard JS, McGhee JD. 2001. Activation of Hypodermal Differentiation in the
952 Caenorhabditis elegans Embryo by GATA Transcription Factors ELT-1 and ELT-3 .
953 *Mol Cell Biol* **21**:2533–2544. doi:10.1128/mcb.21.7.2533-2544.2001
954 Gómez-Saldivar G, Osuna-Luque J, Semple JI, Glauser DA, Jarriault S, Meister P.
955 2020. Tissue-Specific Transcription Footprinting Using RNA. *Genetics* **216**:931–
956 945.
957 Green JL, Inoue T, Sternberg PW. 2008. Opposing Wnt pathways orient cell polarity
958 during organogenesis. *Cell* **134**:646–656. doi:10.1016/j.cell.2008.06.026.Opposing
959 Greenwald IS, Sternberg PW, Robert Horvitz H. 1983. The lin-12 locus specifies cell
960 fates in Caenorhabditis elegans. *Cell* **34**:435–444. doi:10.1016/0092-
961 8674(83)90377-X
962 Hajduskova M, Baytek G, Kolundzic E, Gosdschan A. 2019. MRG-1 / MRG15 Is a
963 Barrier for Germ Cell to Neuron reprogramming. *Genetics* **211**:121–139.
964 Hanahan D. 2022. Hallmarks of Cancer: New Dimensions. *Cancer Discov* 31–47.
965 doi:10.1158/2159-8290.CD-21-1059
966 Hanahan D, Weinberg RA. 2000. The hallmarks of cancer. *Cell* **100**:57–70.
967 doi:10.1007/s00262-010-0968-0
968 Harris TW, Arnaboldi V, Cain S, Chan J, Chen WJ, Cho J, Davis P, Gao S, Grove CA,
969 Kishore R, Lee RYN, Muller HM, Nakamura C, Nuin P, Paulini M, Raciti D, Rodgers
970 FH, Russell M, Schindelman G, Auken K V., Wang Q, Williams G, Wright AJ, Yook
971 K, Howe KL, Schedl T, Stein L, Sternberg PW. 2020. WormBase: A Modern Model
972 Organism Information Resource. *Nucleic Acids Res* **48**:D762–D767.
973 doi:10.1093/nar/gkz920
974 Hills-Muckey K, Martinez MAQ, Stec N, Hebbar S, Saldanha J, Medwig-Kinney TN,
975 Moore FEQ, Ivanova M, Moraro A, Jordan D, Moss EG, Ercan S, Zinovyeva AY,
976 Matus DQ, Christopher M. 2021. An engineered, orthogonal auxin
977 analog/AtTIR1(F79G) pairing improves both specificity and efficacy of the auxin
978 degradation system in Caenorhabditis elegans. *Genetics* iyab174.
979 doi:https://doi.org/10.1093/genetics/iyab174
980 Hoek KS, Eichhoff OM, Schlegel NC, Döbbeling U, Kobert N, Schaerer L, Hemmi S,
981 Dummer R. 2008. In vivo switching of human melanoma cells between proliferative
982 and invasive states. *Cancer Res* **68**:650–656. doi:10.1158/0008-5472.CAN-07-
983 2491
984 Horner MA, Quintin S, Domeier ME, Kimble J, Labouesse M, Mango SE. 1998. pha-4,
985 an HNF-3 homolog, specifies pharyngeal organ identity in Caenorhabditis elegans.
986 *Genes Dev* **12**:1947–1952. doi:10.1101/gad.12.13.1947

Huang G, Jesus B De, Koh A, Blanco S, Rettmann A, Demott E, Sylvester M, Meng C, Waterland S, Rhodes A, Alicea P, Flynn A, Dickinson DJ. 2021. Improved CRISPR / Cas9 knock-in efficiency via the self-excising cassette (SEC) selection method in C . elegans. *Micropublication Biol*.

Irgen-Gioro S, Walling V, Chong S. 2022. Fixation can change the appearance of phase separation in living cells. *bioRxiv*.

Jarriault S, Schwab Y, Greenwald I. 2008. A Caenorhabditis elegans model for epithelial-neuronal transdifferentiation. *Proc Natl Acad Sci* **105**:3790–3795. doi:10.1073/pnas.0712159105

Jiang H, Xu Z, Zhong P, Ren Y, Liang G, Schilling HA, Hu Z, Zhang Y, Wang X, Chen S, Yan Z, Feng J. 2015. Cell cycle and p53 gate the direct conversion of human fibroblasts to dopaminergic neurons. *Nat Commun* **6**. doi:10.1038/ncomms10100

Jin Y, Hoskins R, Horvitz HR. 1994. Control of type-D GABAergic neuron differentiation by C. elegans UNC-30 homeodomain protein. *Nature* **372**:780–783. doi:10.1038/372780a0

Jumper J, Evans R, Pritzel A, Green T, Figurnov M, Ronneberger O, Tunyasuvunakool K, Bates R, Žídek A, Potapenko A, Bridgland A, Meyer C, Kohl SAA, Ballard AJ, Cowie A, Romera-Paredes B, Nikolov S, Jain R, Adler J, Back T, Petersen S, Reiman D, Clancy E, Zielinski M, Steinegger M, Pacholska M, Berghammer T, Bodenstein S, Silver D, Vinyals O, Senior AW, Kavukcuoglu K, Kohli P, Hassabis D. 2021. Highly accurate protein structure prediction with AlphaFold. *Nature* **596**:583–589. doi:10.1038/s41586-021-03819-2

Kagias K, Ahier A, Fischer N, Jarriault S. 2012. Members of the NODE (Nanog and Oct4-associated deacetylase) complex and SOX-2 promote the initiation of a natural cellular reprogramming event in vivo. *Proc Natl Acad Sci U S A* **109**:6596–6601. doi:10.1073/pnas.1117031109

Karp X, Greenwald I. 2003. Post-transcriptional regulation of the E/Daughterless ortholog HLH-2, negative feedback, and birth order bias during the AC/VU decision in C. elegans. *Genes Dev* **17**:3100–3111. doi:10.1101/gad.1160803

Katsanos D, Barkoulas M. 2022. Targeted DamID in C . elegans reveals a direct role for LIN-22 and NHR-25 in antagonizing the epidermal stem cell fate. *Sci Adv* **8**:eabk3141.

Keeley DP, Hastie E, Jayadev R, Kelley LC, Chi Q, Payne SG, Jeger JL, Hoffman BD, Sherwood DR. 2020. Comprehensive Endogenous Tagging of Basement Membrane Components Reveals Dynamic Movement within the Matrix Scaffolding. *Dev Cell* **54**:60-74.e7. doi:10.1016/j.devcel.2020.05.022

Kelley LC, Wang Z, Hagedorn EJ, Wang L, Shen W, Lei S, Johnson SA, Sherwood DR. 2017. Live-cell confocal microscopy and quantitative 4D image analysis of anchor-cell invasion through the basement membrane in Caenorhabditis elegans. *Nat Protoc* **12**:2081–2096. doi:10.1038/nprot.2017.093

Kiefer JC, Smith PA, Mango SE. 2007. PHA-4/FoxA cooperates with TAM-1/TRIM to regulate cell fate restriction in the C. elegans foregut. *Dev Biol* **303**:611–624. doi:10.1016/j.ydbio.2006.11.042

Kimble J, Hirsh D. 1979. The postembryonic cell lineages of the hermaphrodite and male gonads in Caenorhabditis elegans. *Dev Biol* **70**:396–417. doi:10.1016/0012-1606(79)90035-6

1033 Kohrman AQ, Matus DQ. 2017. Divide or Conquer: Cell Cycle Regulation of Invasive
1034 Behavior. *Trends Cell Biol*. doi:10.1016/j.tcb.2016.08.003
1035 Kolundzic E, Ofenbauer A, Bulut SI, Uyar B, Baytek G, Sommermeier A, Seelk S, He M,
1036 Hirsekorn A, Vucicevic D, Akalin A, Diecke S, Lacadie SA, Tursun B. 2018. FACT
1037 Sets a Barrier for Cell Fate Reprogramming in Caenorhabditis elegans and Human
1038 Cells. *Dev Cell* **46**:611-626.e12. doi:10.1016/j.devcel.2018.07.006
1039 Kurashina M, Wang J, Lin J, Lee KK, Johal A, Mizumoto K. 2021. Sustained expression
1040 of unc-4 homeobox gene and unc-37/groucho in postmitotic neurons specifies the
1041 spatial organization of the cholinergic synapses in c. Elegans. *Elife* **10**:1–26.
1042 doi:10.7554/eLife.66011
1043 Larson AG, Elnatan D, Keenen MM, Trnka MJ, Johnston JB, Burlingame AL, Agard DA,
1044 Redding S, Narlikar GJ. 2017. Liquid droplet formation by HP1α suggests a role for
1045 phase separation in heterochromatin. *Nature* **547**:236–240.
1046 doi:10.1038/nature22822
1047 Leyva-Díaz E, Hobert O. 2019. Transcription factor autoregulation is required for
1048 acquisition and maintenance of neuronal identity. *Development* **146**.
1049 doi:10.1242/dev.177378
1050 Li S, Armstrong CM, Bertin N, Ge H, Milstein S, Boxem M, Vidalain PO, Han JDJ,
1051 Chesneau A, Hao T, Goldberg DS, Li N, Martinez M, Rual JF, Lamesch P, Xu L,
1052 Tewari M, Wong SL, Zhang L V., Berriz GF, Jacotot L, Vaglio P, Reboul J,
1053 Hirozane-Kishikawa T, Li Q, Gabel HW, Elewa A, Baumgartner B, Rose DJ, Yu H,
1054 Bosak S, Sequerra R, Fraser A, Mango SE, Saxton WM, Strome S, Van Den
1055 Heuvel S v., Piano F, Vandenhaute J, Sardet C, Gerstein M, Doucette-Stamm L,
1056 Gunsalus KC, Harper JW, Cusick ME, Roth FP, Hill DE, Vidal M. 2004. A Map of
1057 the Interactome Network of the Metazoan C. elegans. *Science (80-)* **303**:540–543.
1058 doi:10.1126/science.1091403
1059 Liang B, Wang J. 2020. EVI1 in leukemia and solid tumors. *Cancers (Basel)* **12**:1–17.
1060 doi:10.3390/cancers12092667
1061 Lim B, Levine MS. 2021. Enhancer-promoter communication: hubs or loops? *Curr Opin*
1062 *Genet Dev* **67**:5–9. doi:10.1016/j.gde.2020.10.001
1063 Ma X, Zhao Z, Xiao L, Xu W, Kou Y, Zhang Y, Wu G, Wang Y, Du Z. 2021. A 4D single-
1064 cell protein atlas of transcription factors delineates spatiotemporal patterning during
1065 embryogenesis. *Nat Methods* **18**:893–902. doi:10.1038/s41592-021-01216-1
1066 Maduro MF, Lin R, Rothman JH. 2002. Dynamics of a developmental switch: Recursive
1067 intracellular and intranuclear redistribution of Caenorhabditis elegans POP-1
1068 parallels Wnt-inhibited transcriptional repression. *Dev Biol* **248**:128–142.
1069 doi:10.1006/dbio.2002.0721
1070 Martinez M, Matus D. 2020. Auxin-mediated Protein Degradation in Caenorhabditis
1071 elegans. *Bio-Protocol* **10**:1–13. doi:10.21769/bioprotoc.3589
1072 Martinez MAQ, Kinney BA, Medwig-Kinney TN, Ashley G, Ragle JM, Johnson L,
1073 Aguilera J, Hammell CM, Ward JD, Matus DQ. 2020. Rapid Degradation of
1074 Caenorhabditis elegans Proteins at Single-Cell Resolution with a Synthetic Auxin.
1075 *G3 Genes, Genomes, Genet* **10**:267–280. doi:10.1534/g3.119.400781
1076 Matus DQ, Li X-Y, Durbin S, Agarwal D, Chi Q, Weiss SJ, Sherwood DR. 2010. In vivo
1077 identification of regulators of cell invasion across basement membranes. *Sci Signal*
1078 **3**:ra35. doi:10.1126/scisignal.2000654

1079 Matus DQ, Lohmer LL, Kelley LC, Schindler AJ, Kohrman AQ, Barkoulas M, Zhang W,
1080 Chi Q, Sherwood DR. 2015. Invasive Cell Fate Requires G1 Cell-Cycle Arrest and
1081 Histone Deacetylase-Mediated Changes in Gene Expression. *Dev Cell* **35**:162–
1082 174. doi:10.1016/j.devcel.2015.10.002
1083 McKim KS, Peters K, Rose AM. 1993. Two Types of Sites Required for Meiotic
1084 Chromosome Pairing in Caenorhabditis elegans. *Genetics* **134**:749–768.
1085 Medwig-Kinney TN, Palmisano NJ, Matus DQ. 2021. Deletion of a putative HDA-1
1086 binding site in the hlh-2 promoter eliminates expression in C. elegans dorsal uterine
1087 cells. *Micropublication Biol* **1**.
1088 Medwig-Kinney TN, Sirota SS, Gibney T V., Pani AM, Matus DQ. 2022. An in vivo
1089 toolkit to visualize endogenous LAG-2/Delta and LIN-12/Notch signaling in C.
1090 elegans. *microPublication Biol*.
1091 Medwig-Kinney TN, Smith JJ, Palmisano NJ, Tank S, Zhang W, Matus DQ. 2020. A
1092 developmental gene regulatory network for C. elegans anchor cell invasion.
1093 *Development* **147**:dev185850. doi:https://doi.org/10.1101/691337
1094 Medwig TN, Matus DQ. 2017. Breaking down barriers: the evolution of cell invasion.
1095 *Curr Opin Genet Dev* **47**:33–40. doi:10.1016/j.gde.2017.08.003
1096 Milde-Langosch K. 2005. The Fos family of transcription factors and their role in
1097 tumourigenesis. *Eur J Cancer* **41**:2449–2461. doi:10.1016/j.ejca.2005.08.008
1098 Mondal C, Gacha-Garay MJ, Larkin K, Adikes R, Di Martino J, Chien C-C, Fraser M,
1099 Eni-aganga I, Agullo-Pascual E, Ozbek U, Naba A, Gaitas A, Fu T-M, Upadhyayula
1100 S, Betzig E, Matus D, Martin BL, Bravo-Cordero JJ. 2021. A Proliferative to
1101 Invasive Switch is Mediated by srGAP1 Downregulation Through the Activation of
1102 TGFβ2 Signaling. *SSRN Electron J* **40**:111358.
1103 doi:https://doi.org/10.1016/j.celrep.2022.111358 ll
1104 Nelson AT, Wang Y, Nelson ER. 2021. TLX, an Orphan Nuclear Receptor with
1105 Emerging Roles in Physiology and Disease. *Endocrinol (United States)* **162**:1–13.
1106 doi:10.1210/endocr/bqab184
1107 Pani AM, Gibney T V., Medwig-Kinney TN, Matus DQ, Goldstein B. 2022. A new toolkit
1108 to visualize and perturb endogenous LIN-12/Notch signaling. *Micropublication Biol*.
1109 Patel T, Hobert O. 2017. Coordinated control of terminal differentiation and restriction of
1110 cellular plasticity. *Elife* **6**:1–26. doi:10.7554/elife.24100
1111 Patel T, Tursun B, Rahe DP, Hobert O. 2012. Removal of Polycomb Repressive
1112 Complex 2 Makes C. elegans Germ Cells Susceptible to Direct Conversion into
1113 Specific Somatic Cell Types. *Cell Rep* **2**:1178–1186.
1114 doi:10.1016/j.celrep.2012.09.020
1115 Peng QY, Zhang QF. 2006. Precise positions of Phoebe determined with CCD image-
1116 overlapping calibration. *Mon Not R Astron Soc* **366**:208–212. doi:10.1186/1471-
1117 2105-7-208
1118 Pflugrad A, Meir JYJ, Barnes TM, Miller DM. 1997. The Groucho-like transcription factor
1119 UNC-37 functions with the neural specificity gene unc-4 to govern motor neuron
1120 identity in C. elegans. *Development* **124**:1699–1709. doi:10.1242/dev.124.9.1699
1121 Phillips BT, Kidd AR, King R, Hardin J, Kimble J. 2007. Reciprocal asymmetry of SYS-
1122 1/β-catenin and POP-1/TCF controls asymmetric divisions in Caenorhabditis
1123 elegans. *Proc Natl Acad Sci U S A* **104**:3231–3236. doi:10.1073/pnas.0611507104
1124 Phillips BT, Kimble J. 2009. A New Look at TCF and β-Catenin through the Lens of a

Divergent C. elegans Wnt Pathway. *Dev Cell* **17**:27–34. doi:10.1016/j.devcel.2009.07.002

Porta-de-la-Riva M, Fontrodona L, Villanueva A, Cerón J. 2012. Basic Caenorhabditis elegans Methods: Synchronization and Observation. *J Vis Exp* 1–9. doi:10.3791/4019

Putnam A, Cassani M, Smith J, Seydoux G. 2019. A gel phase promotes condensation of liquid P granules in Caenorhabditis elegans embryos. *Nat Struct Mol Biol* **26**.

Quintin S, Michaux G, McMahon L, Gansmuller A, Labouesse M. 2001. The Caenorhabditis elegans gene lin-26 can trigger epithelial differentiation without conferring tissue specificity. *Dev Biol* **235**:410–421. doi:10.1006/dbio.2001.0294

Rahe DP, Hobert O. 2019. Restriction of Cellular Plasticity of Differentiated Cells Mediated by Chromatin Modifiers, Transcription Factors and Protein Kinases. *G3: Genes|Genomes|Genetics* **9**:2287–2302. doi:10.1534/g3.119.400328

Reece-Hoyes JS, Deplancke B, Shingles J, Grove CA, Hope IA, Walhout AJM. 2005. A compendium of Caenorhabditis elegans regulatory transcription factors: A resource for mapping transcription regulatory networks. *Genome Biol* **6**. doi:10.1186/gb-2005-6-13-r110

Reece-Hoyes JS, Walhout AJM. 2018. High-efficiency yeast transformation. *Cold Spring Harb Protoc* **2018**:563–568. doi:10.1101/pdb.prot094995

Richard JP, Zuryn S, Fischer N, Pavet V, Vaucamps N, Jarriault S. 2011. Direct in vivo cellular reprogramming involves transition through discrete, non-pluripotent steps. *J Cell Sci* **124**:e1–e1. doi:10.1242/jcs.090043

Riddle MR, Spickard EA, Jevince A, Nguyen KCQ, Hall DH, Joshi PM, Rothman JH. 2016. Transorganogenesis and transdifferentiation in C. elegans are dependent on differentiated cell identity. *Dev Biol* **420**:136–147. doi:10.1016/j.ydbio.2016.09.020

Riddle MR, Weintraub A, Nguyen KCQ, Hall DH, Rothman JH. 2013. Transdifferentiation and remodeling of post-embryonic C. elegans cells by a single transcription factor. *Development* **140**:4844–4849. doi:10.1242/dev.103010

Riva C, Hajduskova M, Gally C, Suman SK, Ahier A, Jarriault S. 2022. A natural transdifferentiation event involving mitosis is empowered by integrating signaling inputs with conserved plasticity factors. *Cell Rep* **40**:111365. doi:10.1016/j.celrep.2022.111365

Rothman J, Jarriault S. 2019. Developmental Plasticity and Cellular Reprogramming. *Genetics* **213**:723–757.

Rual JF, Ceron J, Koreth J, Hao T, Nicot AS, Hirozane-Kishikawa T, Vandenhaute J, Orkin SH, Hill DE, van den Heuvel S, Vidal M. 2004. Toward improving Caenorhabditis elegans phenome mapping with an ORFeome-based RNAi library. *Genome Res* **14**:2162–2168. doi:10.1101/gr.2505604

Sabari BR, Dall'Agnese A, Boija A, Klein IA, Coffey EL, Shrinivas K, Abraham BJ, Hannett NM, Zamudio A V., Manteiga JC, Li CH, Guo YE, Day DS, Schuijers J, Vasile E, Malik S, Hnisz D, Lee TI, Cisse II, Roeder RG, Sharp PA, Chakraborty AK, Young RA. 2018. Coactivator condensation at super-enhancers links phase separation and gene control. *Science (80-)* **361**. doi:10.1126/science.aar3958

Sallee MD, Aydin T, Greenwald I. 2015. Influences of LIN-12/Notch and POP-1/TCF on the Robustness of Ventral Uterine Cell Fate Specification in Caenorhabditis

elegans Gonadogenesis. *G3: Genes|Genomes|Genetics* **5**:2775–2782. doi:10.1534/g3.115.022608

Sallee MD, Greenwald I. 2015. Dimerization-driven degradation of C. elegans and human E proteins. *Genes Dev* **29**:1356–1361. doi:10.1101/gad.261917.115

Sallee MD, Littleford HE, Greenwald I. 2017. A bHLH Code for Sexually Dimorphic Form and Function of the C. elegans Somatic Gonad. *Curr Biol* **27**:1853-1860.e5. doi:10.1016/j.cub.2017.05.059

Schindelin J, Arganda-Carreras I, Frise E, Kaynig V, Longair M, Pietzsch T, Preibisch S, Rueden C, Saalfeld S, Schmid B, Tinevez J-Y, White DJ, Hartenstein V, Eliceiri K, Tomancak P, Cardona A. 2012. Fiji: an open-source platform for biological-image analysis. *Nat Methods* **9**:676–82. doi:10.1038/nmeth.2019

Seydoux G, Greenwald I. 1989. Cell autonomy of lin-12 function in a cell fate decision in C. elegans. *Cell* **57**:1237–1245. doi:10.1016/0092-8674(89)90060-3

Seydoux G, Schedl T, Greenwald I. 1990. Cell-cell interactions prevent a potential inductive interaction between soma and germline in C. elegans. *Cell* **61**:939–951. doi:10.1016/0092-8674(90)90060-R

Sherwood DR, Sternberg PW. 2003. Anchor cell invasion into the vulval epithelium in C. elegans. *Dev Cell* **5**:21–31. doi:10.1016/S1534-5807(03)00168-0

Shetty P, Lo MC, Robertson SM, Lin R. 2005. C. elegans TCF protein, POP-1, converts from repressor to activator as a result of Wnt-induced lowering of nuclear levels. *Dev Biol* **285**:584–592. doi:10.1016/j.ydbio.2005.07.008

Siegfried K, Kimble J. 2002. POP-1 controls axis formation during early gonadogenesis in C. elegans. *Development* **453**:443–453.

Siegfried KR, Kidd AR, Chesney MA, Kimble J. 2004. The sys-1 and sys-3 Genes Cooperate with Wnt Signaling to Establish the Proximal-Distal Axis of the Caenorhabditis elegans Gonad. *Genetics* **166**:171–186. doi:10.1534/genetics.166.1.171

Simonis N, Rual JF, Carvunis AR, Tasan M, Lemmens I, Hirozane-Kishikawa T, Hao T, Sahalie JM, Venkatesan K, Gebreab F, Cevik S, Klitgord N, Fan C, Braun P, Li N, Ayivi-Guedehoussou N, Dann E, Bertin N, Szeto D, Dricot A, Yildirim MA, Lin C, de Smet AS, Kao HL, Simon C, Smolyar A, Ahn JS, Tewari M, Boxem M, Milstein S, Yu H, Dreze M, Vandenhaute J, Gunsalus KC, Cusick ME, Hill DE, Tavernier J, Roth FP, Vidal M. 2009. Empirically controlled mapping of the Caenorhabditis elegans protein-protein interactome network. *Nat Methods* **6**:47–54. doi:10.1038/nmeth.1279

Smith JJ, Xiao Y, Parsan N, Medwig-Kinney TN, Martinez MAQ, Moore FEQ, Palmisano NJ, Kohrman AQ, Chandhok Delos Reyes M, Adikes RC, Liu S, Bracht SA, Zhang W, Wen K, Kratsios P, Matus DQ. 2022. The SWI/SNF chromatin remodeling assemblies BAF and PBAF differentially regulate cell cycle exit and cellular invasion in vivo, PLOS Genetics. doi:10.1371/journal.pgen.1009981

Spencer SL, Cappell SD, Tsai FC, Overton KW, Wang CL, Meyer T. 2013. The proliferation-quiescence decision is controlled by a bifurcation in CDK2 activity at mitotic exit. *Cell* **155**:369–383. doi:10.1016/j.cell.2013.08.062

Strom AR, Emelyanov A V., Mir M, Fyodorov D V., Darzacq X, Karpen GH. 2017. Phase separation drives heterochromatin domain formation. *Nature* **547**:241–245. doi:10.1038/nature22989

1217 Sturm Á, Saskoi É, Tibor K, Weinhardt N, Vellai T. 2018. Highly efficient RNAi and
1218 Cas9-based auto-cloning systems for C. elegans research. *Nucleic Acids Res*
1219 **46**:e105. doi:10.1093/nar/gky516
1220 Sulston JE, Horvitz HR. 1977. Post-embryonic cell lineages of the nematode,
1221 Caenorhabditis elegans. *Dev Biol* **56**:110–156. doi:10.1016/0012-1606(77)90158-0
1222 Treen N, Shimobayashi SF, Eeftens J, Brangwynne CP, Levine M. 2021. Properties of
1223 repression condensates in living Ciona embryos. *Nat Commun* **12**:1–9.
1224 doi:10.1038/s41467-021-21606-5
1225 Tursun B, Patel T, Kratsios P, Hobert O. 2011. Direct Conversion of C. elegans Germ
1226 Cells into Specific Neuron Types. *Science (80-)* **331**:304–309.
1227 van der Horst SEM, Cravo J, Woollard A, Teapal J, Van den Heuvel S. 2019. C .
1228 elegans Runx / CBFβ suppresses POP-1 (TCF) to convert asymmetric to
1229 proliferative division of stem cell-like seam cells. *Development* **146**:1–34.
1230 doi:10.1242/dev.180034
1231 Varadi M, Anyango S, Deshpande M, Nair S, Natassia C, Yordanova G, Yuan D, Stroe
1232 O, Wood G, Laydon A, Žídek A, Green T, Tunyasuvunakool K, Petersen S, Jumper
1233 J, Clancy E, Green R, Vora A, Lutfi M, Figurnov M, Cowie A, Hobbs N, Kohli P,
1234 Kleywegt G, Birney E, Hassabis D, Velankar S. 2022. AlphaFold Protein Structure
1235 Database: massively expanding the structural coverage of protein-sequence space
1236 with high-accuracy models. *Nucleic Acids Res* **50**:D439–D444.
1237 doi:10.1093/nar/gkab1061
1238 Verghese E, Schocken J, Jacob S, Wimer AM, Royce R, Nesmith JE, Baer GM, Clever
1239 S, McCain E, Lakowski B, Wightman B. 2011. The tailless ortholog nhr-67 functions
1240 in the development of the C. elegans ventral uterus. *Dev Biol* **356**:516–528.
1241 doi:10.1016/j.ydbio.2011.06.007
1242 Wang LH, Baker NE. 2015. E Proteins and ID Proteins: Helix-Loop-Helix Partners in
1243 Development and Disease. *Dev Cell* **35**:269–280. doi:10.1016/j.devcel.2015.10.019
1244 Wang S, Tang NH, Lara-Gonzalez P, Zhao Z, Cheerambathur DK, Prevo B, Chisholm
1245 AD, Desai A, Oegema K. 2017. A toolkit for GFP-mediated tissue-specific protein
1246 degradation in C. elegans. *Development* **144**:2694–2701. doi:10.1242/dev.150094
1247 Wickham H. 2016. ggplot2: Elegant Graphics for Data Analysis. Springer-Verlag New
1248 York.
1249 Wilkinson HA, Fitzgerald K, Greenwald I. 1994. Reciprocal changes in expression of the
1250 receptor lin-12 and its ligand lag-2 prior to commitment in a C. elegans cell fate
1251 decision. *Cell* **79**:1187–1198. doi:10.1016/0092-8674(94)90010-8
1252 Zacharias AL, Walton T, Preston E, Murray JI. 2015. Quantitative Differences in Nuclear
1253 β-catenin and TCF Pattern Embryonic Cells in C. elegans. *PLoS Genet* **11**.
1254 doi:10.1371/journal.pgen.1005585
1255 Zhang L, Ward JD, Cheng Z, Dernburg AF. 2015. The auxin-inducible degradation (AID)
1256 system enables versatile conditional protein depletion in C. elegans. *Development*
1257 **142**:4374–4384. doi:10.1242/dev.129635
1258 Zhong W, Sternberg PW. 2006. Genome-Wide Prediction of C. elegans Genetic
1259 Interactions. *Science (80-)* **311**:1481–1484.
1260 Zhu J, Fukushige T, McGhee JD, Rothman JH. 1998. Reprogramming of early
1261 embryonic blastomeres into endodermal progenitors by a Caenorhabditis elegans
1262 GATA factor. *Genes Dev* **12**:3809–3814. doi:10.1101/gad.12.24.3809

1263 Zuryn S, Ahier A, Portoso M, White ER, Morin MC, Margueron R, Jarriault S. 2014.
1264 Sequential histone-modifying activities determine the robustness of
1265 transdifferentiation. *Science (80-)* **345**:826–829. doi:10.1126/science.1255885
1266

Figure 1 Medwig-Kinney et al. (2022)

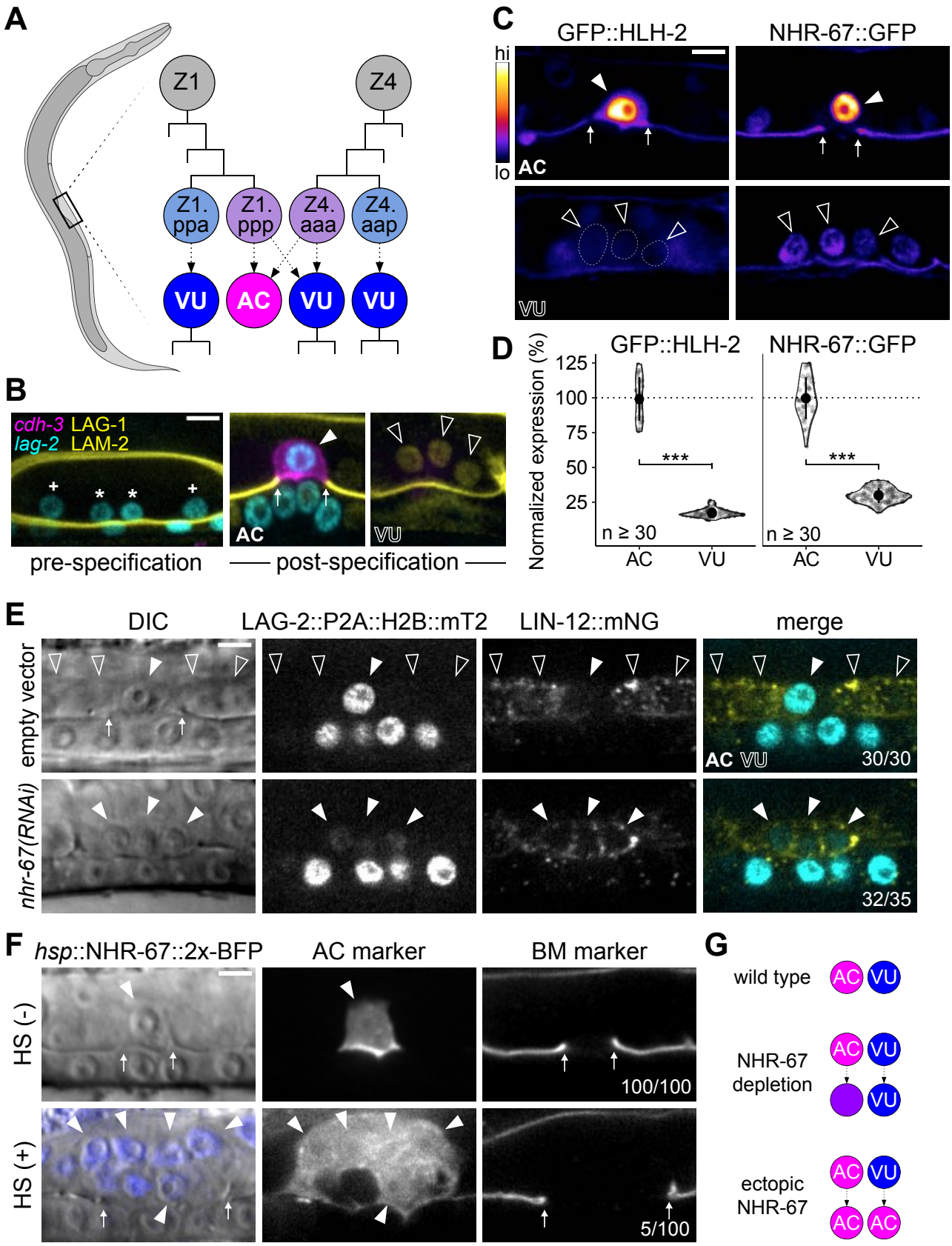

Figure 1–figure supplement 1 Medwig-Kinney et al. (2022)

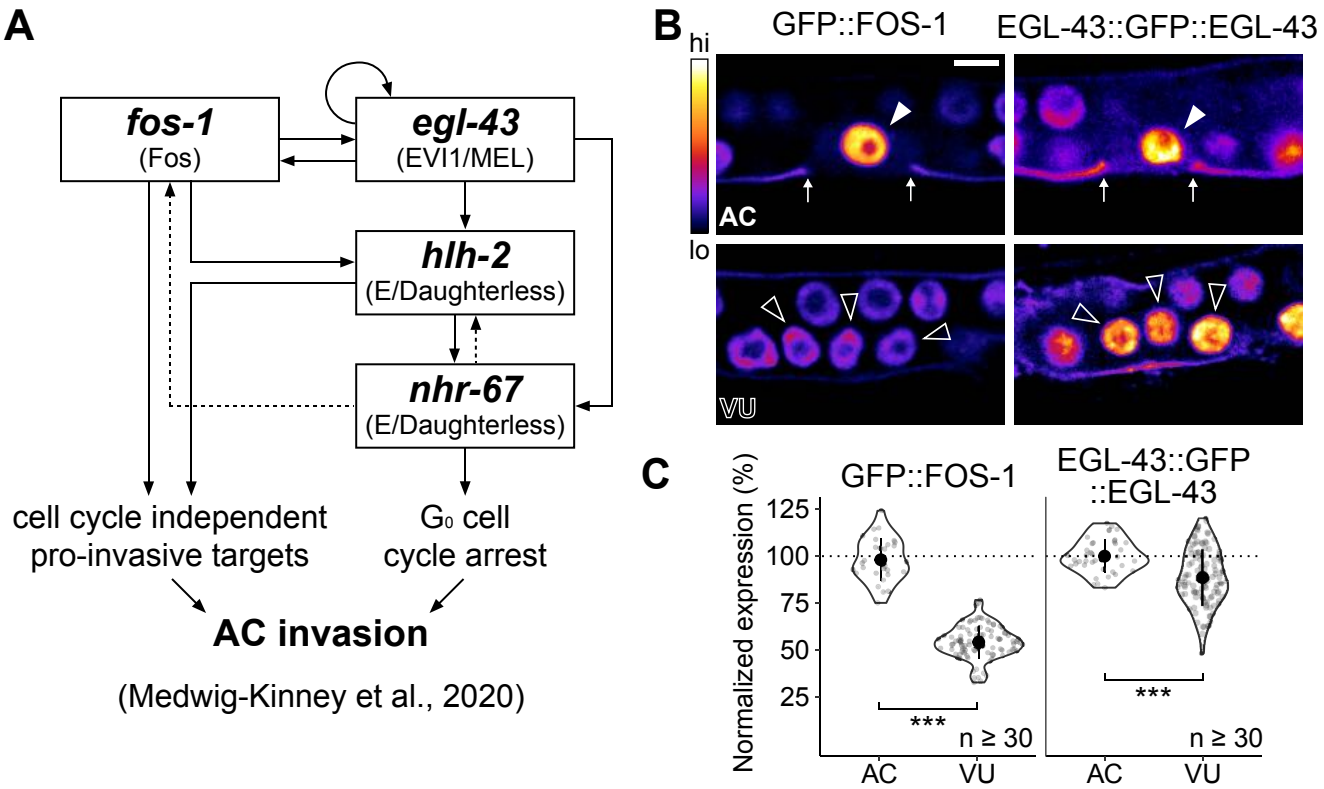

Figure 2 Medwig-Kinney et al. (2022)

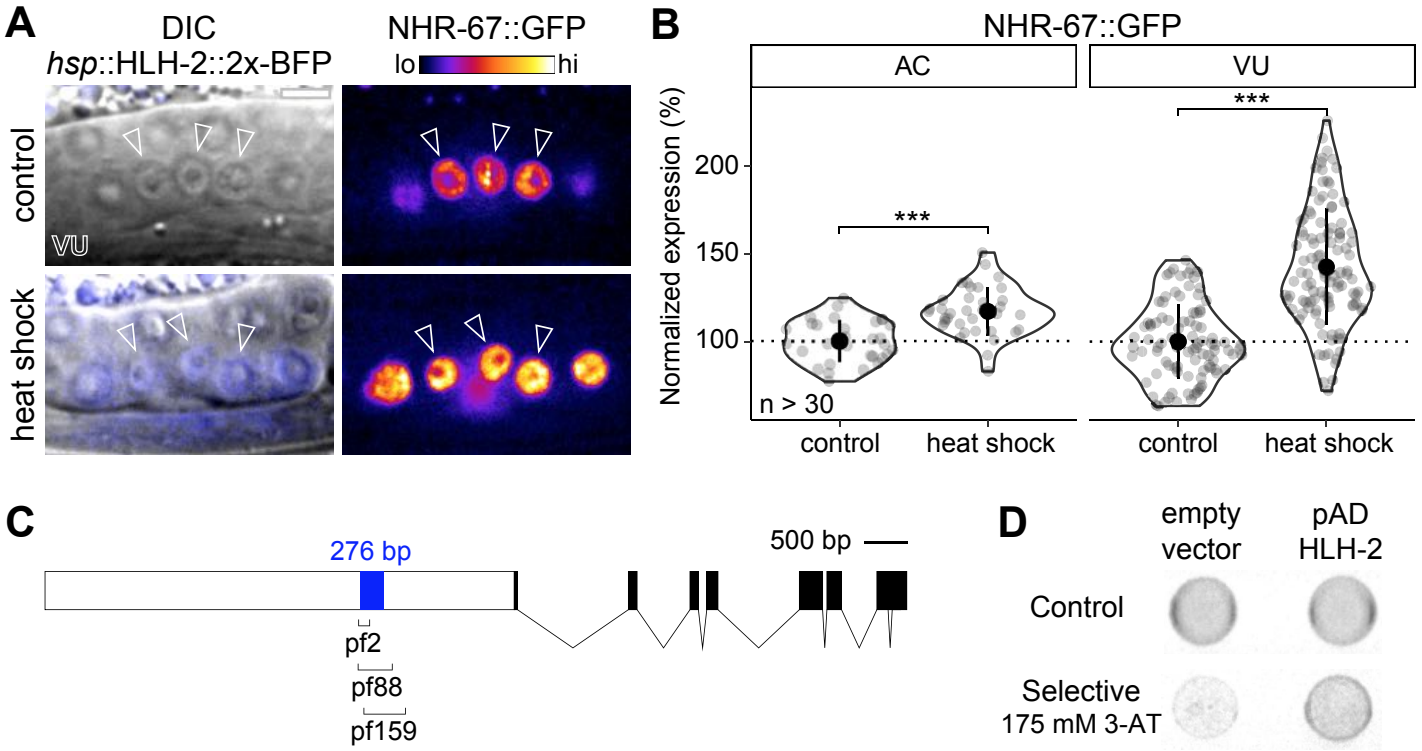

Figure 2–figure supplement 1

Medwig-Kinney et al. (2022)

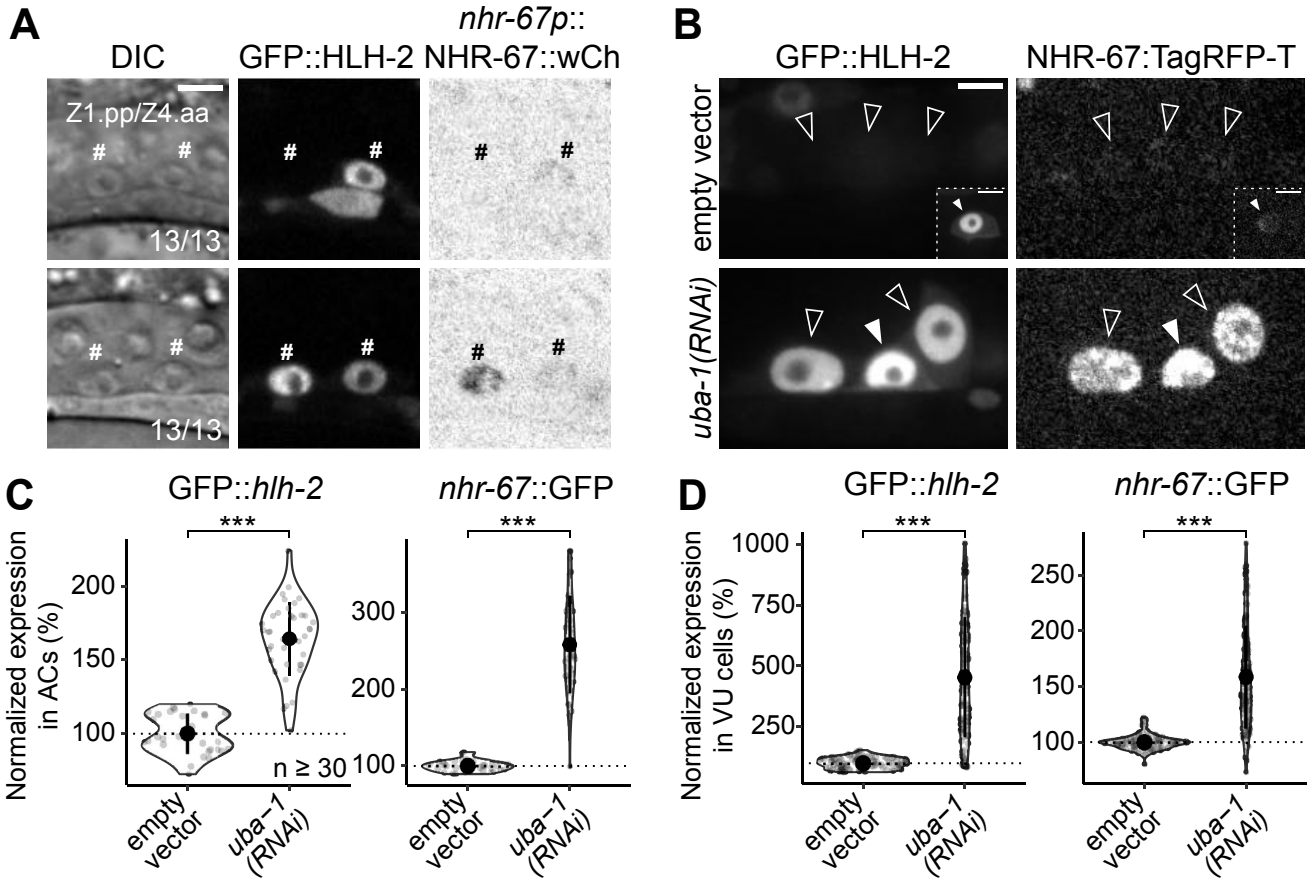

Figure 3

Medwig-Kinney et al. (2022)

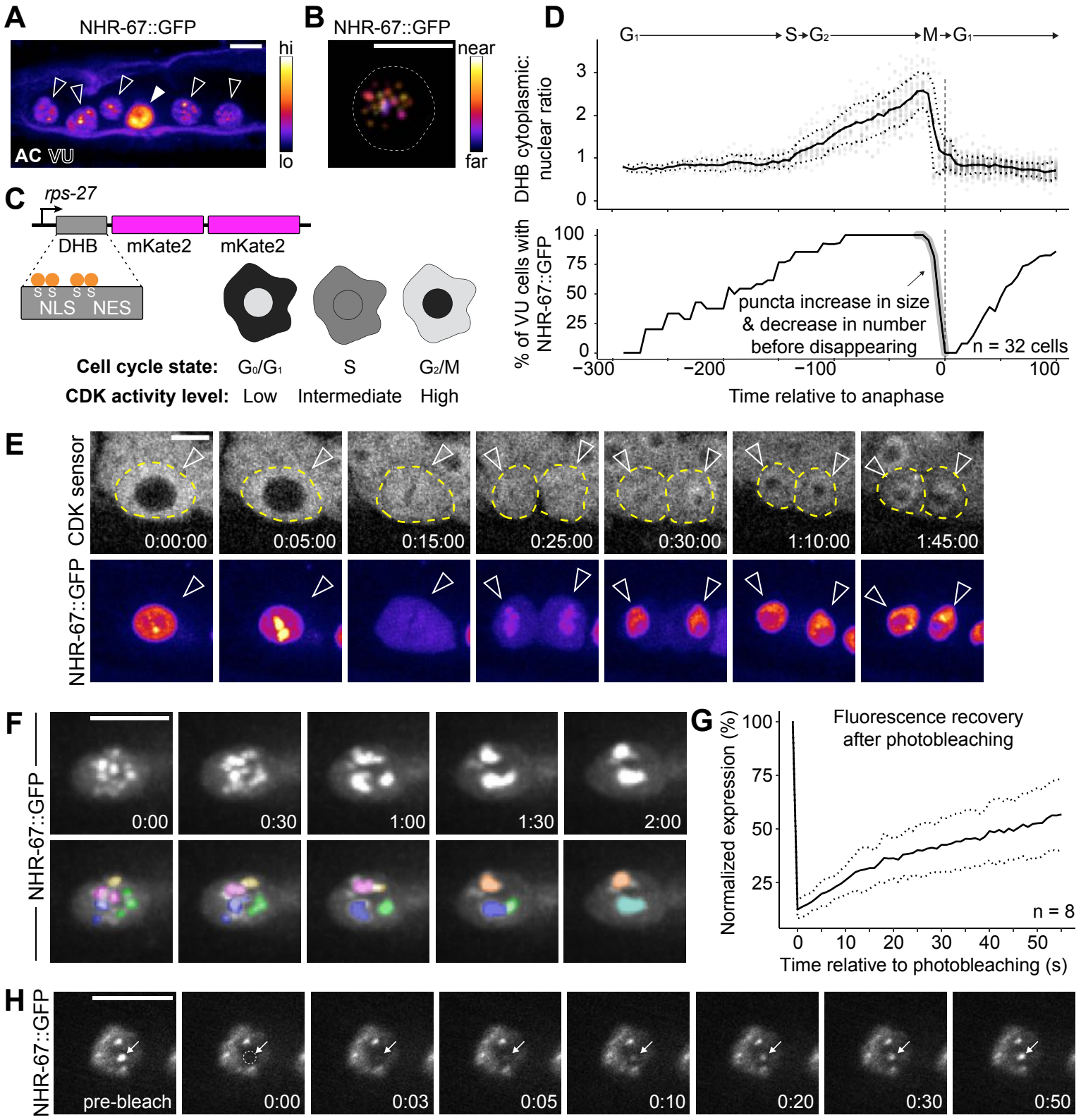

Figure 3–figure supplement 1 Medwig-Kinney et al. (2022)

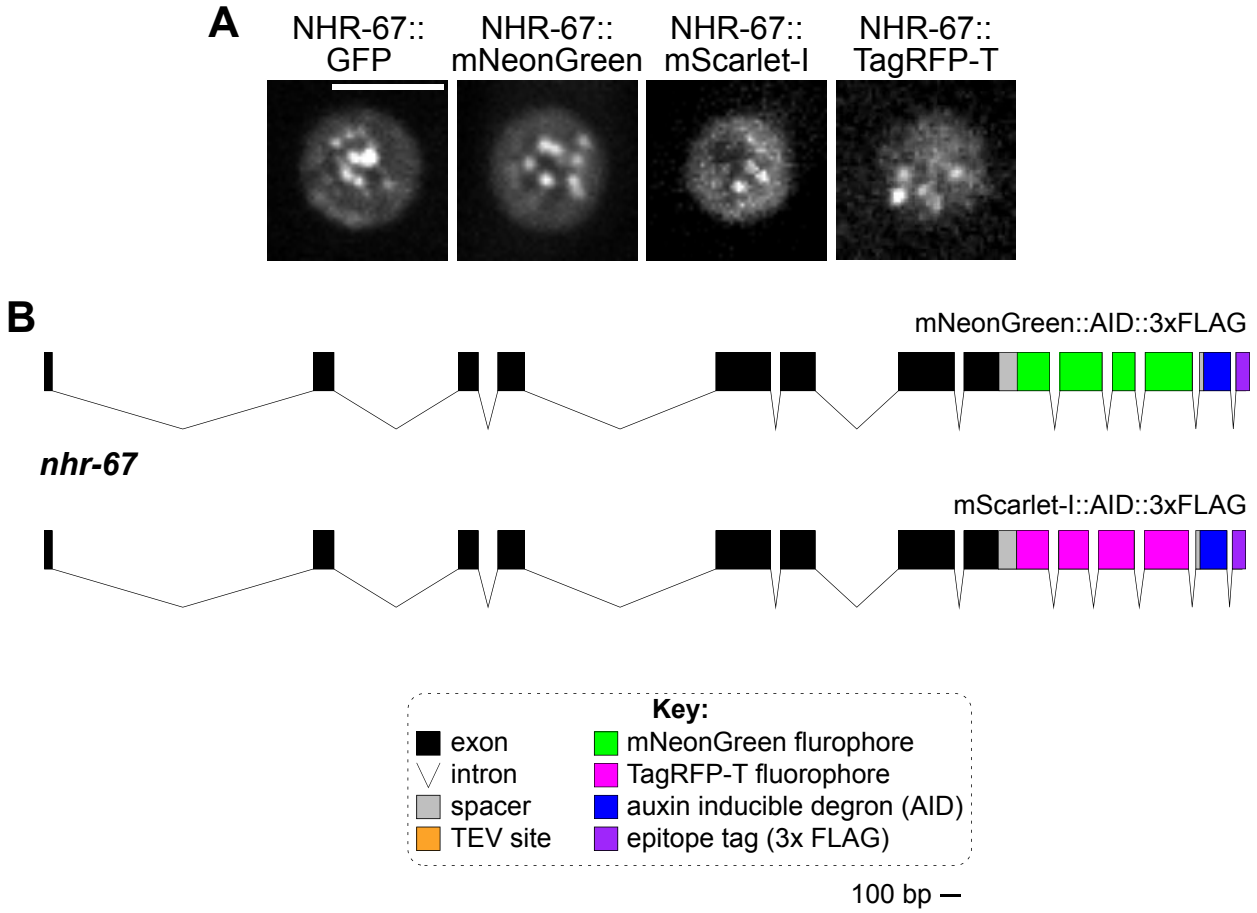

Figure 4 Medwig-Kinney et al. (2022)

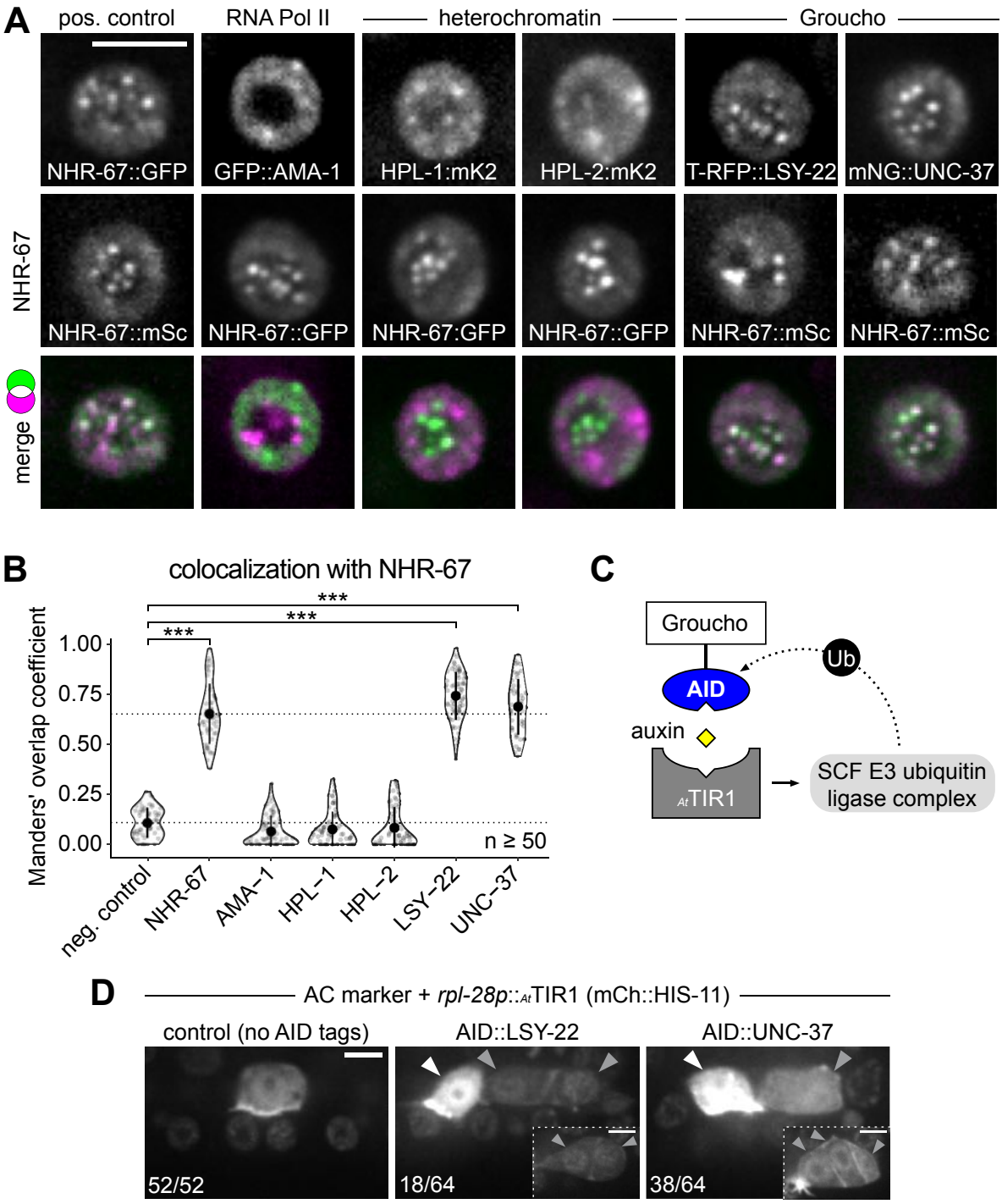

Figure 4–figure supplement 1

Medwig-Kinney et al. (2022)

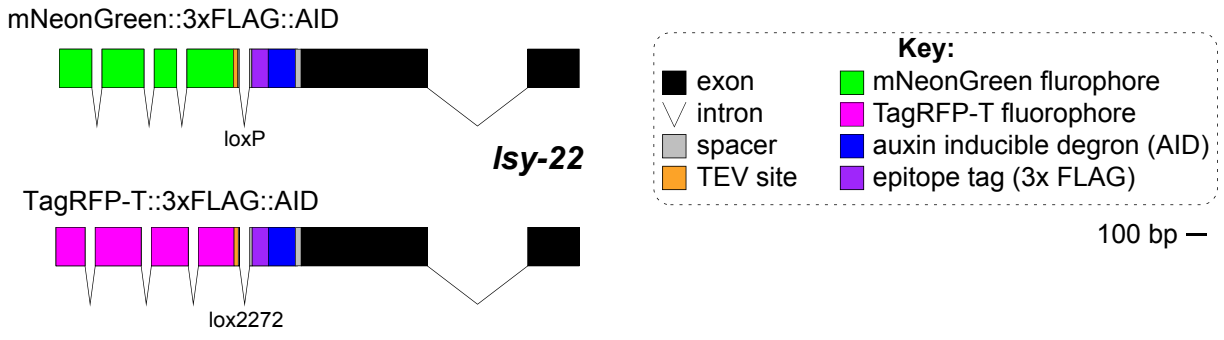

Figure 4–figure supplement 2 Medwig-Kinney et al. (2022)

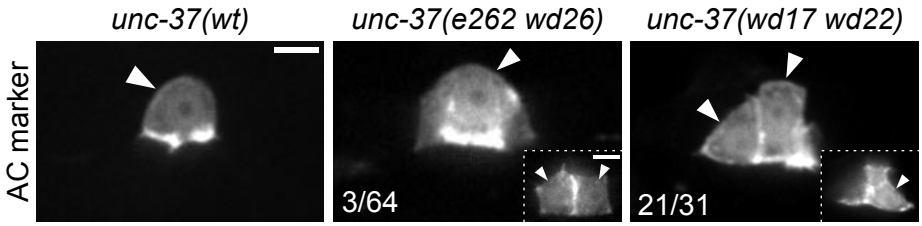

Figure 5 Medwig-Kinney et al. (2022)

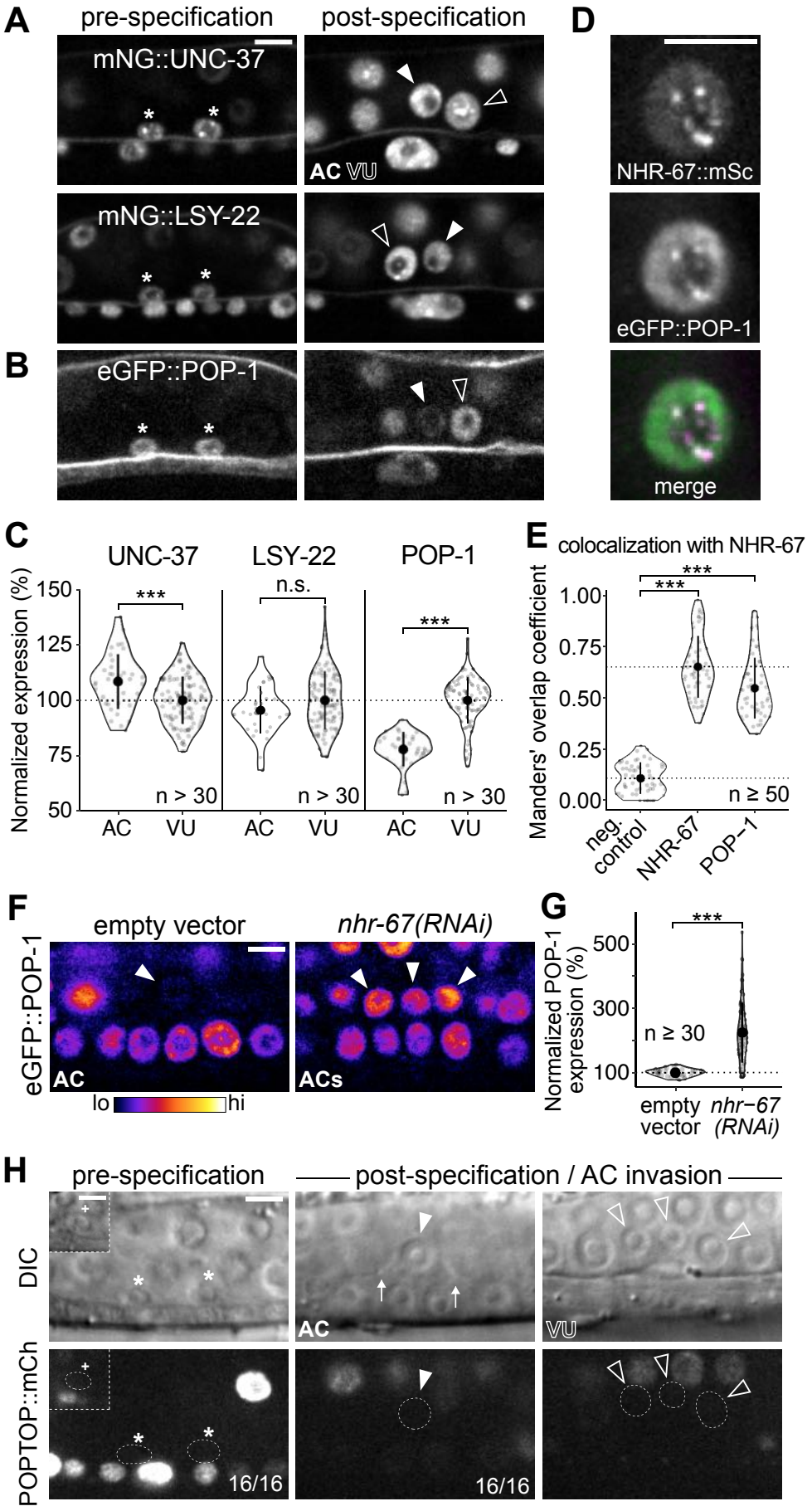

Figure 5–figure supplement 1 Medwig-Kinney et al. (2022)

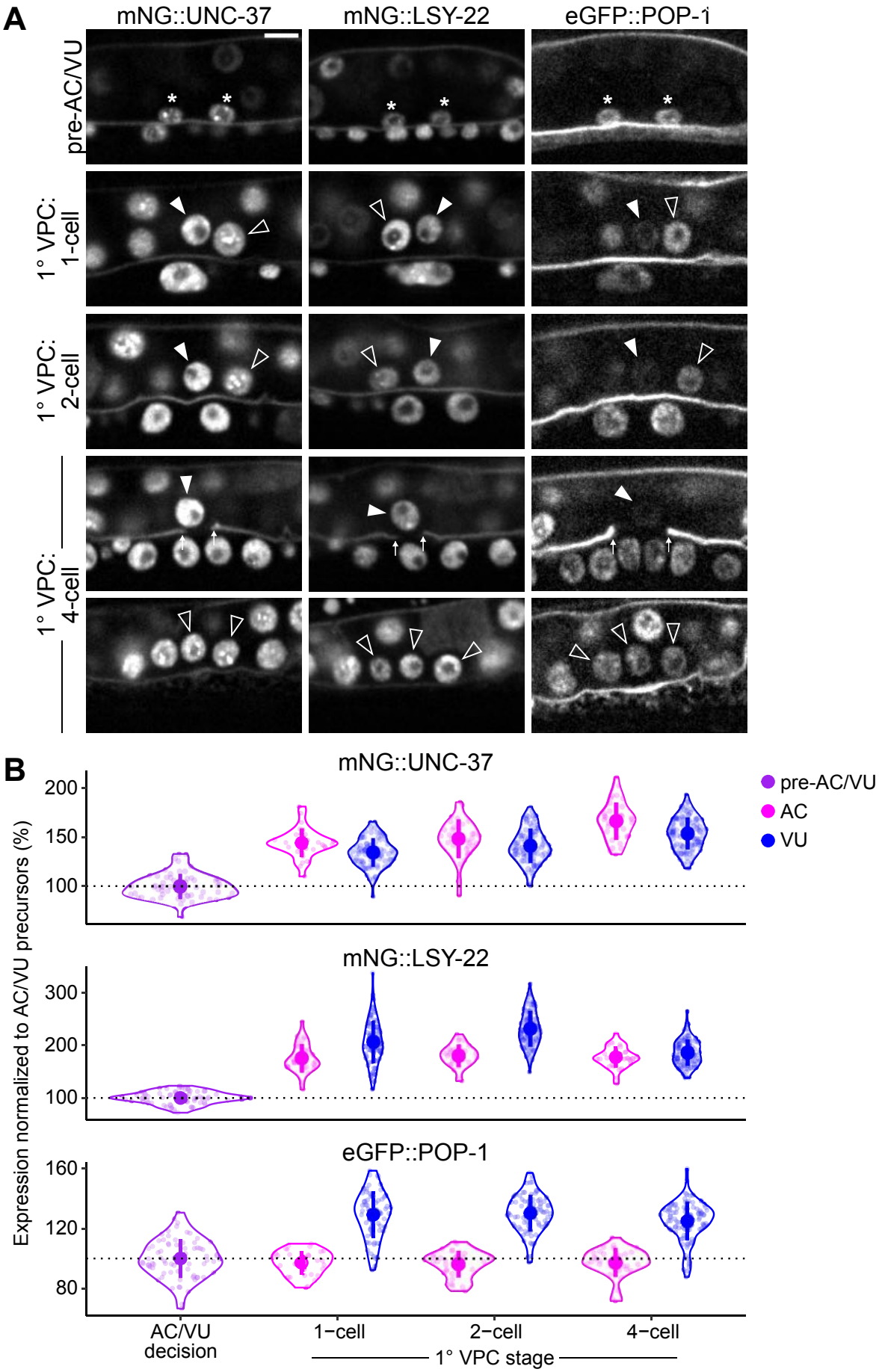

Figure 5–figure supplement 2 Medwig-Kinney et al. (2022)

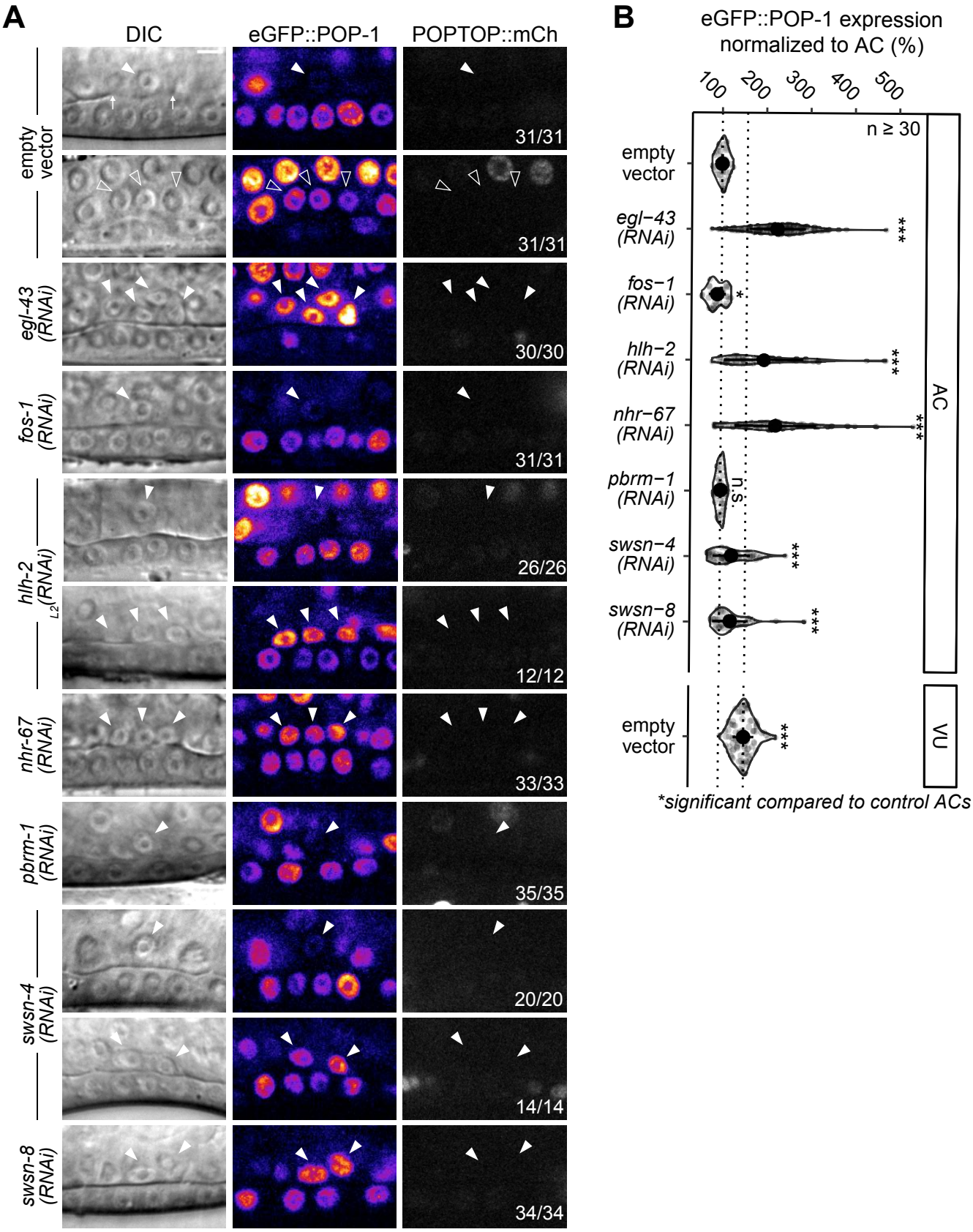

Figure 5–figure supplement 3 Medwig-Kinney et al. (2022)

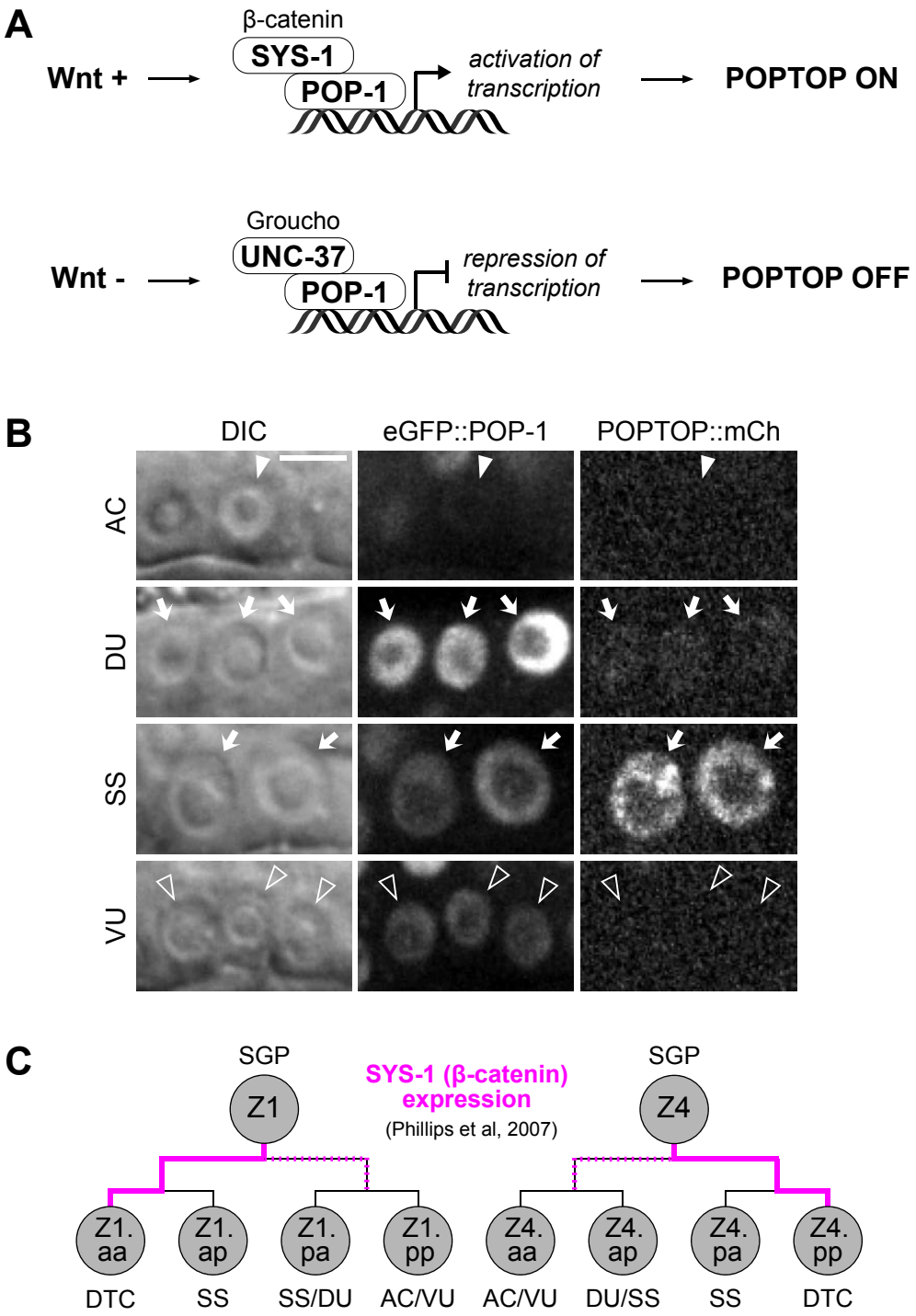

Figure 6 Medwig-Kinney et al. (2022)

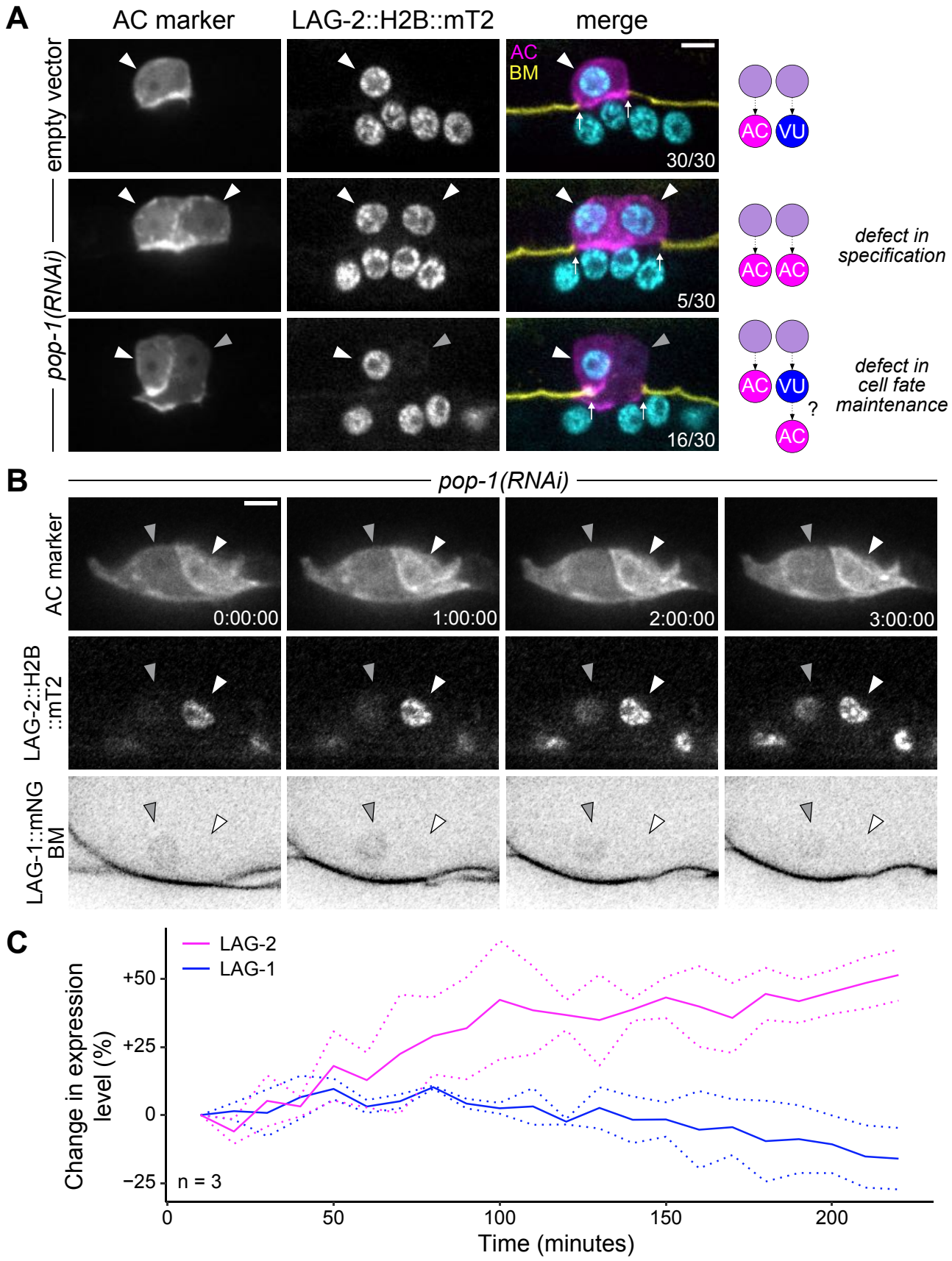

Figure 6–figure supplement 1

Medwig-Kinney et al. (2022)

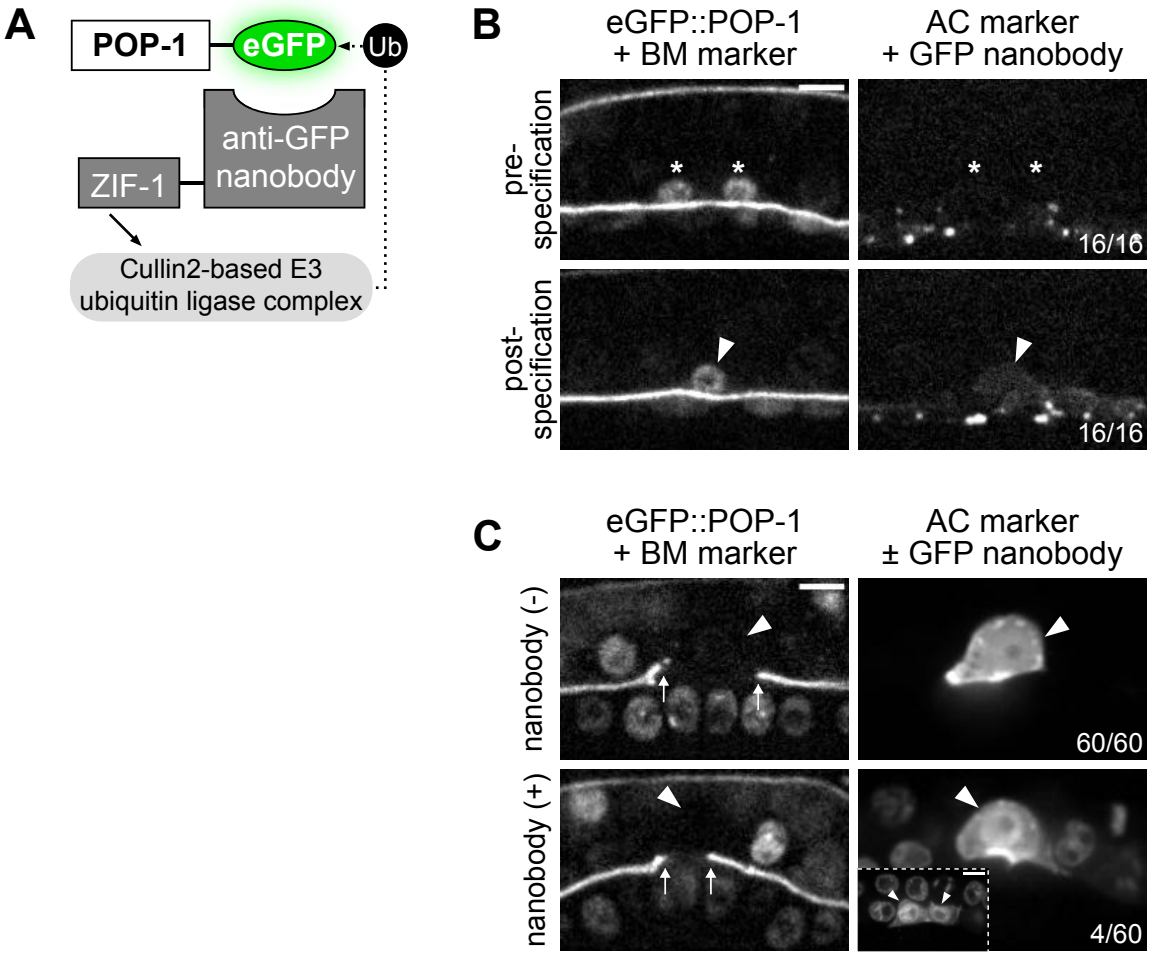

Figure 6–figure supplement 2 Medwig-Kinney et al. (2022)

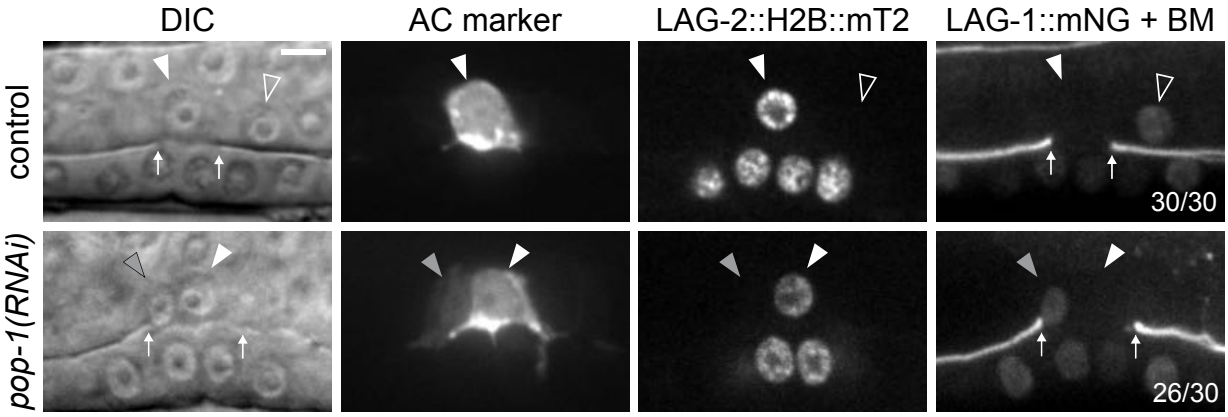

Figure 7 Medwig-Kinney et al. (2022)

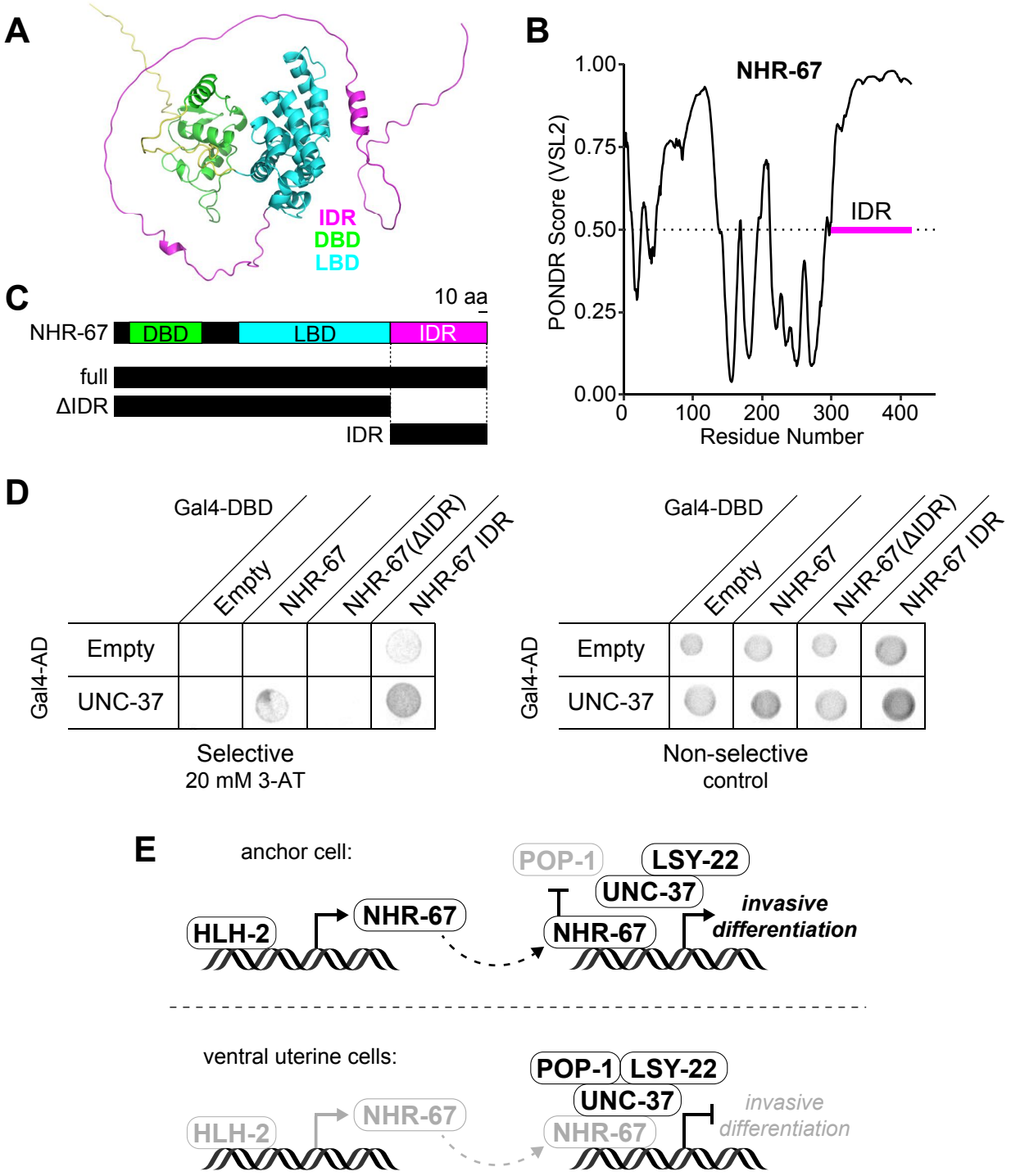
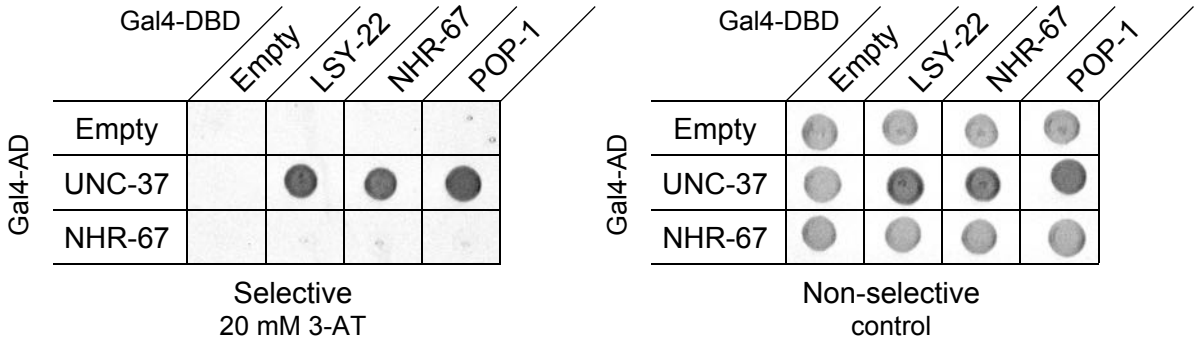
Figure 7–figure supplement 1 Medwig-Kinney et al. (2022)